Third- and fourth-order analysis of the intensities and polarization dependence of two-photon absorption lines of Gd^{3+} in LaF_3 and aqueous solution

M. C. Downer* and A. Bivas†
Division of Applied Sciences, Harvard University, Cambridge, Massachusetts 02138
(Received 19 April 1983)

A comprehensive report and analysis of our observations of numerous parity-allowed direct two-photon transitions within the $4f^7$ configuration of the Gd^{3+} ion is presented. The experimental technique is ultraviolet fluorescence detection following optical excitation with a dye-laser beam. Previous results and analyses are extended in three ways. (1) The intensities and polarization dependence of individual Stark components, in addition to integrated multiplet intensities, are reported and analyzed for Gd^{3+}:LaF_3. In those cases ($^8S_{7/2}\rightarrow{}^6P_{5/2}, {}^6D_{9/2,3/2,5/2}$) where a second-order theory of two-photon absorption adequately explains the integrated intensity, it also (with the exception of $^6D_{9/2}$) explains the Stark-component intensities. The remaining transitions are anomalously strong, and in some cases violate the angular momentum selection rules $\Delta L, \Delta J \leq 2$ and exhibit strong anisotropies, in contradiction to the second-order theory. It is shown that introduction of third- and fourth-order contributions involving spin-orbit and/or crystal-field interactions among levels of the $4f^6 5d$ configuration, which serve as intermediate states, can account for both the integrated and Stark-component intensities of these transitions. (2) The strong anisotropy observed for the transitions $^8S_{7/2}\rightarrow{}^6P_{3/2}, {}^6I_J, {}^6D_{1/2}$ in Gd^{3+}:LaF_3 is explained quantitatively as a polarization-dependent interference between contributions to the intensity which are comparable in magnitude. Interference is destructive for $\vec{E}\|\hat{z}$ and constructive for $\vec{E}\perp\hat{z}$, creating an order-of-magnitude contrast in the line strength for the two polarizations. (3) A two-photon excitation spectrum of Gd^{3+} in aqueous solution is reported. Linewidths comparable to those of room-temperature solids and Stark splittings which suggest a low-symmetry quasistatic environment are observed.

I. INTRODUCTION

Two-photon spectroscopy began in 1961 with the pioneering experiment of Kaiser and Garrett,[1] in which a broad ultraviolet band arising from a $4f^7\rightarrow 4f^6 5d$ transition was excited in Eu^{2+}:CaF_2 using the red light from a pulsed ruby laser. Bayer and Schaak[2] later investigated the polarization dependence of this interconfigurational two-photon transition at several discrete excitation frequencies. With the development of tunable dye lasers, the sharp parity-allowed $4f^N\rightarrow 4f^N$ transitions of rare-earth ions in solids became accessible to observation by two-photon absorption (TPA), although for a number of years only a few such transitions were observed.[3–5] Recently, however, we reported extensive observations[6–8] of the relative intensities and polarization dependence of numerous intra-$4f^7$ two-photon transitions in Gd^{3+}:LaF_3 using both continuous-wave[6] (cw) and pulsed[7] dye-laser excitation.

These observations have provoked considerable theoretical interest[7–9] because of their very strong disagreement with predictions of the standard theory of lanthanide transition intensities developed by Judd[10] and Ofelt[11] for one-photon absorption, and modified by Axe[12] to apply to two-photon processes. In particular, the experimental results displayed a threefold anomaly. (1) Several transitions ($^8S_{7/2}\rightarrow{}^6I_{13/2,15/2,17/2}, {}^6D_{1/2}$) violated the angular momentum selection rule $\Delta J \leq 2$; in most cases J mixing of $4f^7$ levels proved inadequate to explain this behavior. Furthermore, some transitions violated the selection rules $\Delta S = 0$ and $\Delta L \leq 2$ to a much greater extent than the use of intermediate coupled initial- and final-state wave functions could explain. (2) Such transitions were anomalously strong with respect to the predictions of a second-order theory,[12] as well as (3) strongly anisotropic, or dependent on direction of polarization with respect to crystalline axes.

Judd and Pooler[9] showed that by expanding Axe's second-order theory[12] of two-photon absorption to include third-order terms involving the spin-orbit interaction among levels of the intermediate configurations (principally $4f^6 5d$), the anomalous intensity observed[6] for $^8S_{7/2}\rightarrow{}^6P_{7/2}$ in Gd^{3+} could be explained because the spin selection rule breaks down in third order. Downer *et al.*[7,8] have shown that third-order terms involving the crystal-field interaction among intermediate states can explain much of the anomalous intensity of the six $^8S_{7/2}\rightarrow{}^6I_J$ lines in Gd^{3+}:LaF_3, since the selection rules $\Delta L, \Delta J \leq 2$ then break down. A general theoretical treatment[8] of these third-order contributions to TPA, as well as fourth-order contributions to TPA and third-order contributions to one-photon absorption, is planned to be presented in a forthcoming theoretical paper.

The main purpose of the present paper is to present and analyze the experimental results for Gd^{3+}:LaF_3 in considerably greater detail than has been done in a previous publication.[7] In addition, new results on the two-photon excitation spectrum of Gd^{3+} in aqueous solution are described which represent the first observation of intra-$4f^N$ two-

photon absorption in a rare-earth aqueous solution. Section II outlines the experimental procedure based on ultraviolet fluorescence detection. Section III reviews the previously reported[7] results on the integrated intensities of 14 $f^7 \rightarrow f^7$ two-photon transitions in Gd^{3+}:LaF_3 and presents new data on the polarization dependence of the individual Stark components in the crystalline sample, which were fully resolved in all scans, and on the two-photon spectrum of the aqueous solution sample. The analysis of single-photon electric dipole intensities in lanthanides has generally been confined to the integrated intensities of transitions between J multiplets observed with unpolarized light (e.g., Carnall *et al.*[13]), since the complex theoretical expressions which come into play are greatly simplified by summing over M_J values and polarization directions.[10,11] By contrast the theoretical prediction of the two-photon intensities of Stark components for any specified polarization in a crystalline sample is quite simple and involves no unknown odd-parity crystal parameters, so the comparison of the theoretical and experimental intensities is straightforward. In the case of three excited J multiplets of Gd^{3+}:LaF_3 ($^6P_{5/2}$,$^6D_{5/2,7/2}$), crystal-field energy-level calculations[14] have left some Stark-component assignments ambiguous. Analysis of the polarization dependence of the two-photon intensities, however, resolves these ambiguities, allowing definite assignments of all components to be made. Section IV analyzes the integrated and Stark-component intensities for Gd^{3+}:LaF_3 in terms of second-, third-, and fourth-order contributions to TPA. It is shown that the strong anisotropies previously observed,[7] but not explained, in the integrated intensities of $^8S_{7/2} \rightarrow {}^6P_{3/2}, {}^6I_J, {}^6D_{1/2}$ can be explained quantitatively as polarization-dependent interference among the various contributions to TPA.

II. EXPERIMENTAL PROCEDURE

Many significant details of the experimental apparatus and procedure have been described previously,[6,7] and will be reviewed and supplemented here. While some early measurements[6] employed cw dye-laser (Coherent model 599-21) excitation, most measurements[7] were performed with a pulsed nitrogen-laser–pumped dye laser of the Hänsch type (repetition rate approximately 10 Hz, pulses typically 0.1 mJ, 5 nsec) which afforded high peak intensity and wider frequency tunability. The frequency bandwidth (approximately 0.5 cm^{-1}) was less than the homogeneous linewidth of most absorption lines at 80 K (2–3 cm^{-1}), the temperature at which most recordings were taken, so no further narrowing with intracavity etalons was necessary. A single laser beam, with polarization controlled by means of a Glan prism and variable retarder, was focused tightly (typically $f=1$ cm) into the sample. A small portion of the beam was directed into a 1-m Jarrell-Ash spectrometer for frequency calibration. A 0.5-mol.% Gd^{3+}:LaF_3 sample obtained from Optovac, Inc. was mounted on the cold finger of a cryostat cooled to liquid-nitrogen or, when desired, liquid-helium temperature. The crystalline c axis was oriented either parallel or perpendicular to $\vec{S}$ (Poynting vector) and the following polarizations of the excitation were examined: (1) $\vec{S}||\hat{c}$, $\vec{E}\perp\hat{c}$, and $\vec{E}$ rotated in the c plane; (2) $\vec{S}||\hat{c}$, circular polarization; (3) $\vec{S}\perp\hat{c}$,$\vec{E}||\hat{c}$. These are the only polarizations which can propagate through the birefringent crystal without change. Gd^{3+} enters LaF_3 in a single type of substitution site possessing approximately D_{3h} symmetry,[14] with the site-symmetry axis parallel to $\hat{c}$, although ESR,[15] Raman scattering,[16] and neutron-diffraction[17] studies indicate slight distortions to a lower, probably C_{2v}, symmetry. Aqueous solutions of Gd^{3+} were prepared by dissolving 99.9%-pure gadolinium oxide (Gd_2O_3) powder in dilute perchloric acid at various concentrations between 0.5 and 1.0M.

Two-photon transitions were induced between the $4f^7$ $^8S_{7/2}$ ground state and the 14 excited states shown in Fig. 1, which belong to the ^6P_J, ^6I_J, and ^6D_J groups of $4f^7$. Since the lowest excited states lie at 32 000 cm^{-1}, there are no near-resonant intermediate states for optical excitation frequencies. In fact, the levels which play the role of intermediate states belong primarily to the far off-resonant $4f^6 5d$ configuration, which lies at an average energy of about 150 000 cm^{-1} above the ground state. uv fluorescence from one-photon relaxation back to the ground state was collected at right angles to the excitation beam with a suitably filtered EMI 9635QB photomultiplier tube, and this signal was processed by a boxcar integration system.

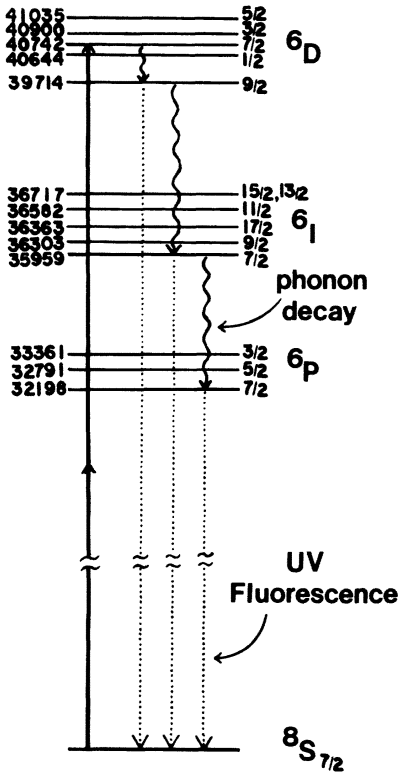

FIG. 1. Diagram of lowest-energy $4f^7$ levels of Gd^{3+}:LaF_3 showing two-photon excitation of $^6D_{7/2}$ and subsequent decay by phonon emission and fluorescence. Numbers at left give average energy of each J multiplet in cm^{-1}. Levels of $4f^6 5d$ begin at about 78 000 cm^{-1}.

Fluorescence following two-photon excitation emerges from Gd^{3+}:LaF_3 with a lifetime of nearly 10 msec at the wavelengths 3100, 2800, and 2500 Å in the branching ratio 6:1:3, corresponding to the relaxation of $^6P_{7/2}$, $^6I_{7/2}$, and $^6D_{9/2}$ directly to the ground state. Total fluorescence yield is essentially unity because the large energy gap separating $^6P_{7/2}$ from the ground state prevents nonradiative decay. In the aqueous solution fluorescence was observed only at 3100 Å, indicating that higher excited states decay nonradiatively to $^6P_{7/2}$ before fluorescence is emitted. Even the 3100-Å fluorescence was partially quenched, since the fluorescent lifetime shortened to about 2 msec and observed integrated fluorescence signals were weaker than those from a crystalline sample of comparable dopant concentration. For both samples, however, the proportionality of TPA to fluorescent intensity was checked by comparing single-photon absorption and excitation spectra from 30000 to 42000 cm^{-1} taken with a Cary 14 spectrophotometer. The relative single-photon intensities agreed in the two spectra. Munir *et al.*[18] have observed nonlinear optical absorption in rare-earth-doped glasses using optoacoustic detection, which may supplement fluorescence detection for the study of weakly or nonfluorescing lanthanide ions.

Variations in the temporal and spatial characteristics of the laser beam from a pulsed source can introduce sizable errors into the measurement of absolute nonlinear absorption intensities,[19] although the measurements of relative cross sections required in the present study are less severely affected. Nevertheless, a number of precautions were observed. Continual boxcar averaging of fluorescence signals from 20 to 30 laser shots minimized the effect of random pulse variations. Measurements of the $^8S_{7/2} \rightarrow {}^6P_J$ transition intensity ratios were checked with both a well-characterized cw transverse electromagnetic (TEM_{00}) excitation beam[6] and the pulsed source, yielding results which agreed to within 10%, and indicating that systematic pulse variations played little role within the gain curve of a single laser dye. Systematic variations can become more pronounced with wide frequency tuning and changes of the laser dye. Since our measurements employed three dyes (Rhodamine B, Pilot 495, and Coumarin 500), measurements with each dye were referenced to the second harmonic generated in a quartz plate[20,21] by a reference beam split from the excitation beam. Because second-harmonic generation depends on intensity in the same way as TPA, spatial and temporal pulse variations affect the two processes in the same way.

The experimental error entering measurements of the relative integrated intensities of two transitions was roughly proportional to the frequency spacing between them. We estimate that our measurements of the relative intensity of one multiplet for two different polarizations of the excitation beam are accurate to $\pm 10\%$, of the relative intensity of two closely spaced multiplets to $\pm 30\%$, and of the relative intensity of widely separated multiplets which must be excited using different laser dyes to plus or minus a factor of 2.5. Checks were made for systematic errors by using different samples, different lasers, different optics (particulary different degrees of focusing into the sample), and different sample temperatures. Results from multiple scans were averaged to improve statistics, and cross checks of measured intensity ratios were made to confirm internal consistency.

A rough measurement was made of the absolute TPA cross section of Gd^{3+}:LaF_3 using the TEM_{00} cw beam tuned to one-half the frequency of the peak of the middle Stark component of $^6P_{5/2}$ at 80 K, where the fullwidth at half maximum (FWHM) of this line was about 3 cm^{-1}. A cross section of 2×10^{-55} cm^4 sec/photon ion (0.6×10^{-36} cm^4/W ion), which agrees within a factor of 3 with a cross section calculated[8] using a second-order theory, was measured. In obtaining the experimental value, unity fluorescence yield and isotropic fluorescence emission were assumed, as was a thin-lens approximation in determining the size of the interaction region. Further details of the experimental apparatus and procedure are given in Ref. 8.

III. EXPERIMENTAL RESULTS

A. Gd^{3+}:LaF_3

Experimental two-photon excitation recordings for a number of transitions in Gd^{3+}:LaF_3 at 80 K for three polarizations of the excitation beam are presented in Figs. 2—8. Recordings for other observed transitions are included in Ref. 8. The vertical axes of all of these figures indicate the normalized two-photon absorption intensity in arbitrary units on the same internally consistent scale. The scale of Figs. 9—11 is also internally consistent; the smaller numbers were chosen to reflect the smaller fluorescent signals observed from the solution sample, but their relation to the scale used for the crystalline sample is a rough estimate only.

The level positions of all Stark components of the 14 excited multiplets of Gd^{3+}:LaF_3 observed were measured to within ± 1 cm^{-1}, and agreed with those reported by Schwiesow, and Crosswhite[22] and by Carnall, Fields, and Sarup[23] for the linear absorption spectrum. Three of the observed levels ($^6D_{1/2,3/2,5/2}$) has been predicted, but not observed, in the one-photon absorption (OPA) spectrum of Gd^{3+}:LaF_3, although the last two have been observed in other hexagonal crystals.[24] $^6D_{1/2}$ is extremely weak in OPA, while $^6D_{3/2,5/2}$, as observed in TPA, are exceptionally broad (15—20 cm^{-1} FWHM) compared to other lines at 80 K, and thus have correspondingly lower peak intensities. These lines narrowed only slightly at liquid-helium temperature. The observation of these lines attests to the high signal discrimination obtainable with fluorescence detection of TPA.

The bar graph in Fig. 12 presents the two-photon absorption line strengths for Gd^{3+}:LaF_3 on an arbitrary logarithmic scale. Each vertical bar represents the intensity for a particular polarization of the excitation beam of a J multiplet integrated over $J+\frac{1}{2}$ Stark components. The first vertical bar for each transition refers to $\vec{E}\perp\hat{c}$ regardless of the orientation of $\vec{E}$ in the c plane, since all observed transitions were isotropic in the c plane. The horizontal lines in Fig. 12 denote relative intensities predicted by the second-order theory of Axe,[12] where the best fit has been made to the four transition intensities

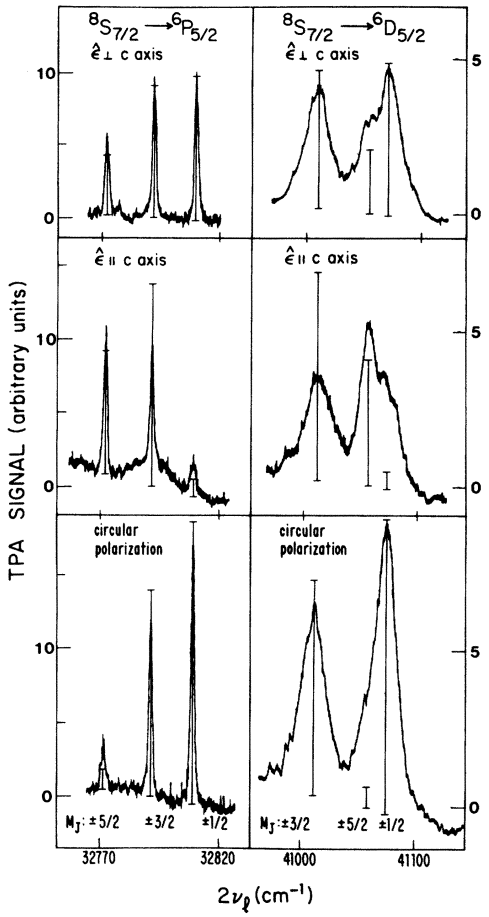

FIG. 2. Experimental two-photon excitation recordings of $^6P_{5/2}$ and $^6D_{5/2}$ in Gd^{3+}:LaF_3 showing polarization dependence of the individual excited-state Stark components. Stark splitting of $^8S_{7/2}$ ground state was not resolved. Vertical bars show predictions of a second-order theory of two-photon absorption, assuming D_{3h} site symmetry and neglecting J mixing.

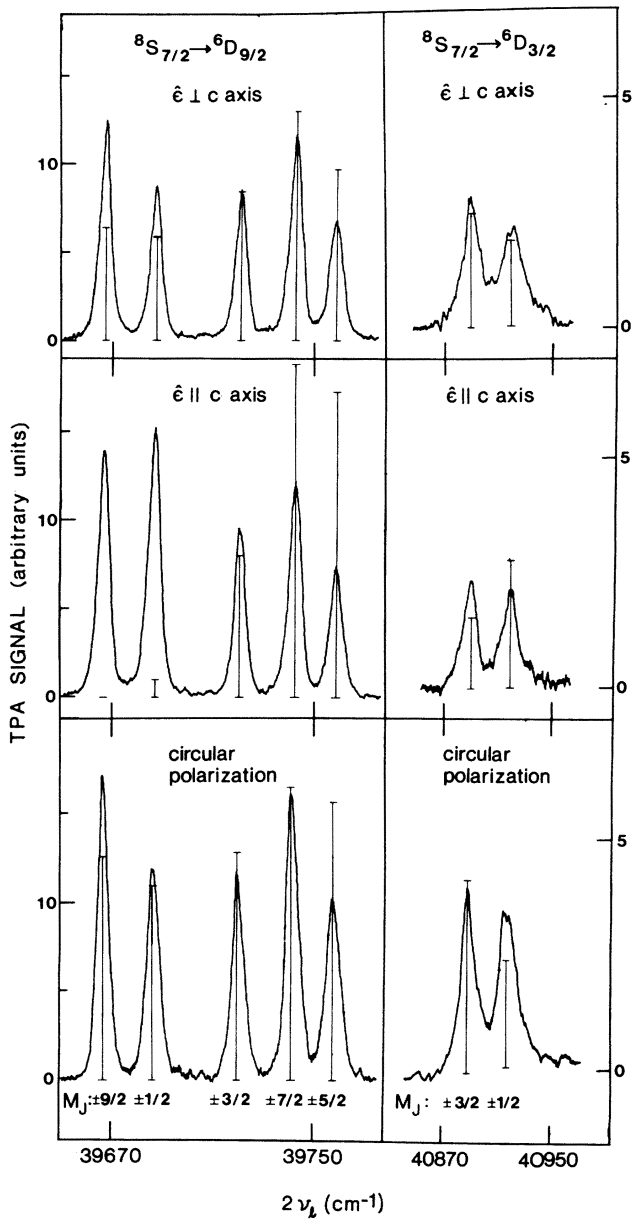

FIG. 3. Experimental two-photon excitation recordings of $^6D_{9/2}$ and $^6D_{3/2}$. Theoretical annotation is the same as in Fig. 2.

$^8S_{7/2} \rightarrow {}^6P_{5/2}, {}^6D_{9/2,3/2,5/2}$, which are the only transitions which agree both in relative intensities and polarization dependence with the Axe predictions.

The remaining transitions exhibit enormous discrepancies with the second-order theory. The predictions for the ^6I_J lines fall well below the scale of Fig. 12, in marked disagreement with the experimental results shown. In fact, the second-order theory predicts zero intensity for $^8S_{7/2} \rightarrow {}^6I_{13/2,15/2,17/2}$ because of the selection rule $\Delta J \leq 2$ for TPA. Furthermore, these "forbidden" transitions are stronger than neighboring "allowed" transitions. The second-order predictions for the allowed $^8S_{7/2} \rightarrow {}^6I_{7/2,9/2,11/2}$ transitions, though nonzero, are still too small by several orders of magnitude to explain the observed intensities. In these cases, the approximate selection rule $\Delta L \leq 2$ is still violated. All of the ^6I_J intensities depend strongly on the direction of linear polarization, as indicated by the order-of-magnitude difference in the heights of the first two vertical bars for these transitions. These transitions therefore exhibit a threefold discrepancy with the second-order theory: selection-rule violation, strong anisotropy, and anomalously strong intensities.

The $^6P_{7/2}$ line is unique in that the cross section for linear polarization, though isotropic, is about 12 times stronger than for circular polarization, in direct contradiction to the Axe theory. The cross section for circular polarization is, however, in fair agreement with the second-order theory. To a much smaller extent, the same isotropic enhancement for linear polarization is evident in $^8S_{7/2} \rightarrow {}^6D_{7/2}$.

The weak $^6P_{3/2}$ and $^6D_{1/2}$ lines show strong anisotropy of a form which closely resembles that of the ^6I_J lines. As shown below, the explanation of this anisotropy is the same in all cases. $^8S_{7/2} \rightarrow {}^6D_{1/2}$ constitutes a fourth case of violation of the $\Delta J \leq 2$ selection rule. The intensity of

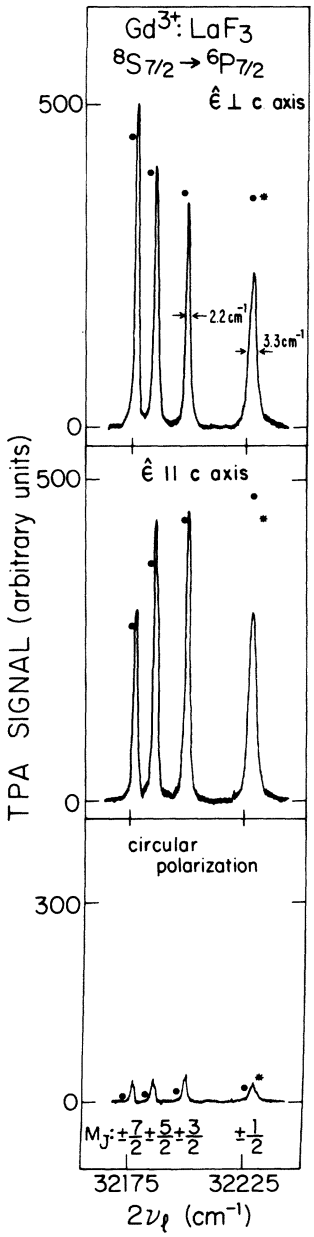

FIG. 4. Experimental two-photon excitation recordings of $^6P_{7/2}$ in Gd^{3+}:LaF_3 for three polarizations of the excitation beam. Closed circles show Stark-component intensities predicted by including third-order terms involving the spin-orbit interaction among intermediate states belonging to the $4f^6 5d$ configuration along with the standard second-order contribution to two-photon absorption. The $M=\pm\frac{1}{2}$ component is broadened more than the other components by spontaneous phonon emission. The asterisk (*) indicates the height this component would have if it were equal in width to the other three components.

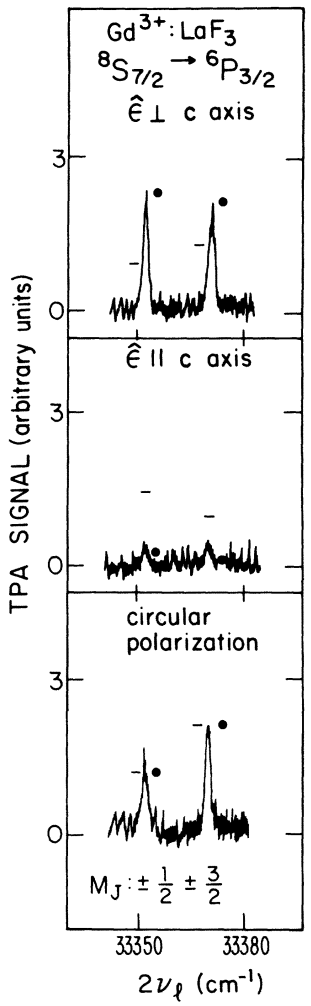

FIG. 5. Experimental two-photon excitation recording of $^6P_{3/2}$ in Gd^{3+}:LaF_3 for three polarizations of the excitation beam. Horizontal lines show Stark-component intensities predicted by including third-order terms involving the spin-orbit interaction along with the second-order term, but neglecting the admixture of $^6P_{7/2}$ in the $^6P_{3/2}$ wave function. Closed circles show revised theoretical intensities when this admixture is taken into account.

$^6P_{3/2}$ for $\vec{E}\perp\hat{c}$ and circular polarization is several times stronger than the second-order prediction.

The data in Figs. 2–8 show a marked polarization dependence in the intensities of individual Stark components, even in those cases where the integrated intensity is isotropic. These variations are analyzed in detail in Sec. IV.

B. Gd^{3+} in aqueous solution

We have observed the same 14 two-photon transitions $^8S_{7/2}\rightarrow{}^6P_J,{}^6I_J,{}^6D_J$ for Gd^{3+} in an aqueous solution. Concentrations of $0.5M$ were necessary to obtain sizable TPA signals, although some of the stronger lines could be observed at lower concentrations. Giuliani[25] reported experimental evidence for competing one- and two-photon processes in pumping the charge-transfer band of aqueous europium perchlorate solutions. The present results, however, constitute the first observation of two-photon $f^N\rightarrow f^N$ transitions in rare-earth solutions.

The relative integrated intensities of the various transitions were measured in the same manner as for the crys-

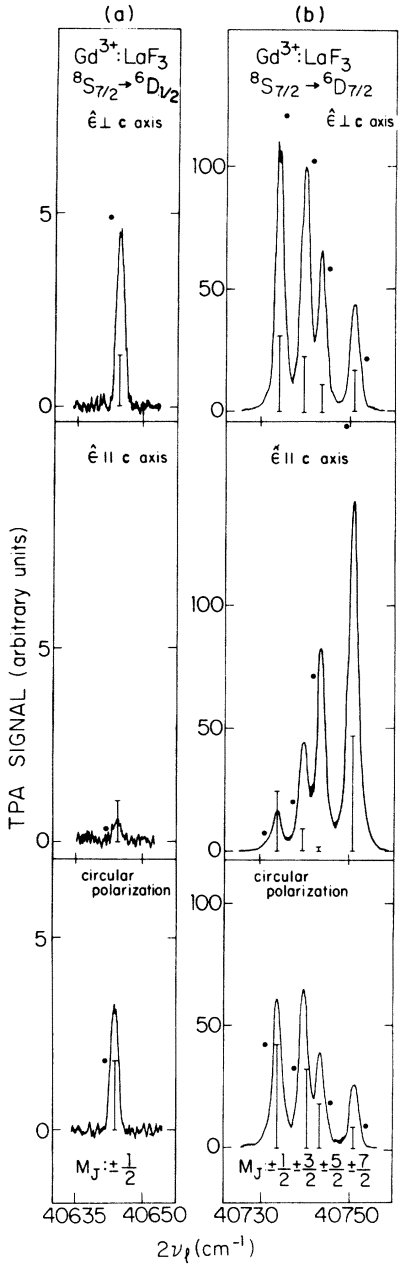

FIG. 6. Two-photon excitation recordings of (a) $^6D_{1/2}$ and (b) $^6D_{7/2}$ in $Gd^{3+}:LaF_3$ for three polarizations of the excitation beam. Vertical bars show intensities predicted by second-order theory alone, closed circles by combined action of second-order terms, and third-order terms involving the spin-orbit interaction.

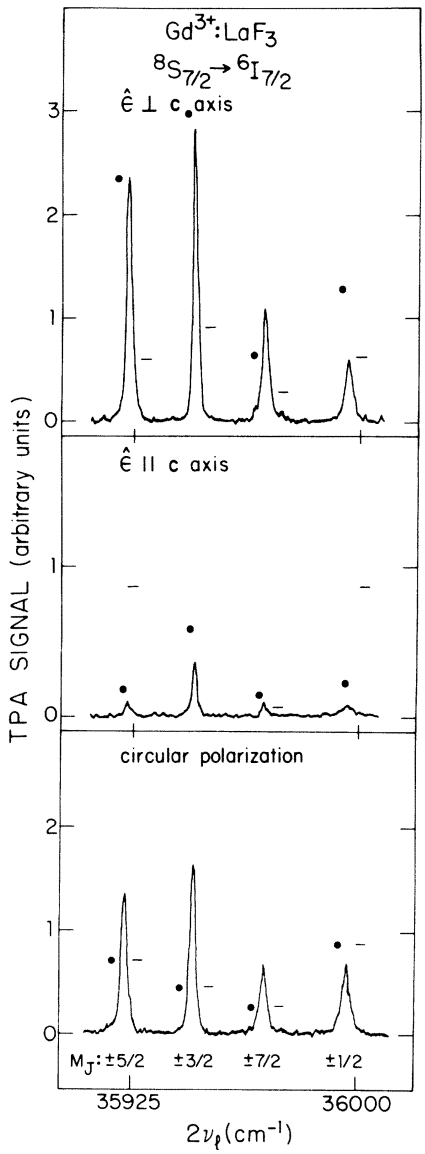

FIG. 7. Experimental two-photon excitation recordings of $^6I_{7/2}$ in $Gd^{3+}:LaF_3$ for three polarizations of the excitation beam. Closed circles show intensities predicted by the combined action of the third-order contribution in the crystal-field, the fourth-order contribution, and the third-order scalar contribution in the spin-orbit interaction acting upon the $^6P_{7/2}$ admixture in the $^6I_{7/2}$ wave function. Horizontal lines show intensities predicted when the $^6P_{7/2}$ admixture is neglected. For $\vec{E}||\hat{z}$ and $M = \pm\frac{3}{2}$, this calculated value falls at 2.7 on the vertical scale in the middle panel and is not shown.

talline sample using a linearly or a circularly polarized excitation beam. The results were consistent with those for $Gd^{3+}:LaF_3$ within experimental error. The anisotropies observed for the $^6P_{3/2}$, ^6I_J, and $^6D_{1/2}$ lines in the crystal were, of course, not observed in solution because the ions are randomly oriented. In these cases, the observed line strength for linear polarization was within a factor of 3 of the average of the line strengths observed for $\vec{E} \perp \hat{c}$ and $\vec{E}||\hat{c}$ in the crystal, relative to the remaining line strengths. For $^6P_{7/2}$, $^6D_{3/2,5/2,7/2,9/2}$, the ratio S(linear)/S(circular) confirmed the ratio observed in the crystal. In particular, the intensity of $^6P_{7/2}$ was over 10 times weaker for circular polarization (see Fig. 9), while $^6D_{3/2,5/2}$ (see Fig. 11) and $^6D_{9/2}$ showed a small enhancement for circular polarization. $^6D_{7/2}$ had nearly the same intensity for both polarizations.

The two-photon excitation recordings in Figs. 9—11 show clearly resolved Stark splittings, similar to crystal-field splittings observed in solid hosts, indicating the presence of a quasistatic hydration complex, or "iceberg,"[26]

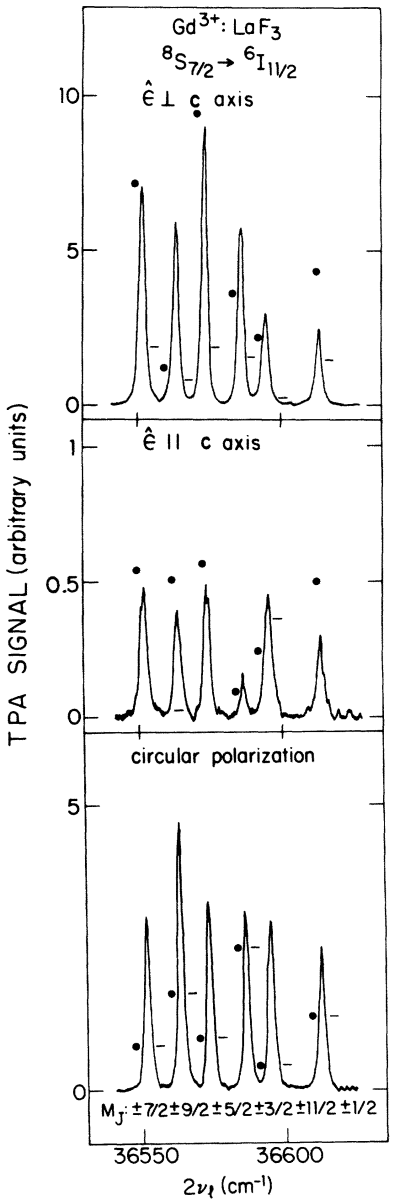

FIG. 8. Experimental two-photon excitation recordings of $^6I_{11/2}$ in Gd^{3+}:LaF_3. Theoretical annotation is the same as in Fig. 7. For $\vec{E}\|\hat{z}$, most of the horizontal lines, indicating intensities predicted when the $^6P_{7/2}$ admixture is neglected, fall above the scale of the middle recording, and are not shown. Specifically, they fall at the values 2.9 for $M=\pm\frac{1}{2}$, 1.4 for $M=\pm\frac{3}{2}$, 5.8 for $M=\pm\frac{5}{2}$, and 4.6 for $M=\pm\frac{7}{2}$.

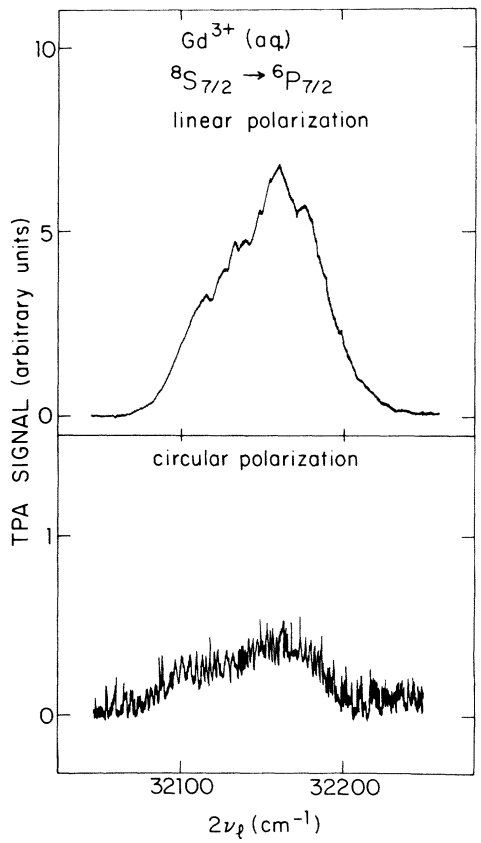

FIG. 9. Experimental two-photon excitation recordings of $^6P_{7/2}$ for Gd^{3+} in aqueous perchlorate solution. Note the appearance of four shoulders in the scan for linear polarization corresponding to four Stark components.

surrounding the cation. Similar splittings were observed long ago in the single-photon absorption and emission spectra of the aqueous[27] as well as anhydrous alcoholic[28] solutions of europium salts, although only very recently were the Stark-component level positions of three multiplets in a number of dilute room-temperature Gd^{3+} solutions reported.[29] In Table I, we report the Stark-component levels of Gd^{3+} in a room-temperature perchlorate solution for a great many more excited multiplets. The splitting is extensively resolved for the ^6P and ^6D levels, although most of the ^6I levels were too closely spaced to reveal much structure. Our observed level positions for $^6P_{7/2,5/2}$ agree within experimental error with those reported by Svoronos *et al.*[29] for the OPA spectrum of Gd^{3+} in a 0.1M perchlorate solution. In addition, the Stark splittings of these and the ^6D levels closely resemble those observed[30] in a frozen Gd^{3+} perchlorate solution at 4 K, indicating that the immediate environment of the ion in solution remains virtually unchanged upon freezing. The barycenters, however, are shifted 10—20 cm^{-1} toward the red at 4 K. Sayre *et al.*[28] observed a similar red shift of about 5 cm^{-1} in the Eu^{3+} solution spectra upon cooling from room temperature to dry-ice temperature. The shift probably results from a larger nephelauxetic effect[31] at the lower temperatures rather than from the vibronic mechanisms operative in crystalline hosts,[32] which generally result in blue shifts upon cooling.

Figures 10 and 11 show that $^6P_{5/2,3/2}$,$^6D_{5/2,3/2}$ split into the maximum number of components allowed by Kramers degeneracy, namely $J+\frac{1}{2}$. The splitting of $^6P_{7/2}$ is not resolved, but four shoulders are discernible in the $^6P_{7/2}$ recording in Fig. 9. The site symmetry at the Gd^{3+} ion is therefore less than cubic. The precise symmetry and structure of the hydration complex, however, has been the

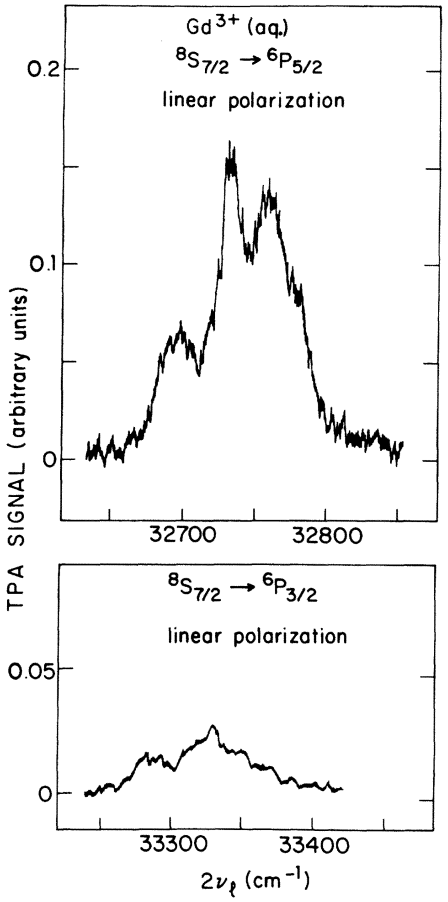

FIG. 10. Experimental two-photon excitation recordings of $^6P_{5/2,3/2}$ for Gd^{3+} in aqueous perchlorate solution showing distinct Stark splittings.

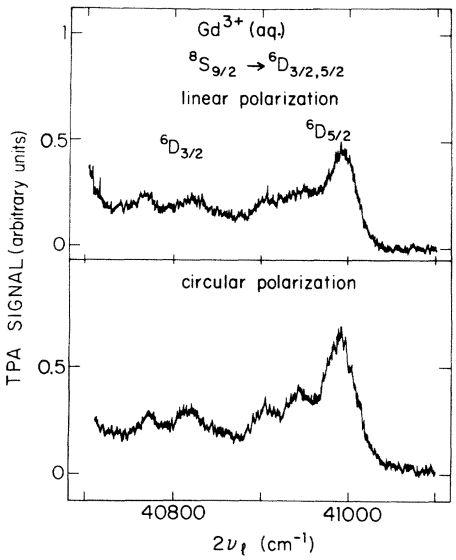

FIG. 11. Experimental two-photon excitation recordings of $^6D_{3/2,5/2}$ for Gd^{3+} in aqueous perchlorate solution.

subject of considerable debate. Recent x-ray-diffraction studies[33] of concentrated rare-earth chloride solutions have established the coordination numbers of most of the lanthanide hydration complexes. Optical spectra have provided valuable clues to the symmetry of the complex. Sayre *et al.*[28] determined that the symmetry of the Eu^{3+} complex was D_{2h} in aqueous solutions and C_{2v} in anhydrous alcohols. Svoronos *et al.*[29] pointed out that the splittings observed for $^6P_{7/2,5/2}$ of Gd^{3+} in aqueous solutions required the presence of a sizable $B_2^{(2)}$ crystal-field parameter, thereby limiting the possible symmetry to C_{2v} or lower. Couture[30] has proposed an eightfold coordinated square antiprism of symmetry D_{4d} for the structure of the surrounding water molecules in the frozen Gd^{3+} perchlorate solution, although a dodecahedral structure has also been suggested.[34] The large number of observed Stark-component levels available from the present spectrum should now permit a meaningful theoretical crystal-field calculation to be made. Hopefully such a calculation could distinguish between the various proposed structures. In addition, the present results demonstrate the feasibility of studing the rare-earth solutions by two-photon absorption using two beams of independently variable polarization. Such studies could provide sufficient information to determine the symmetry of the observed Stark components.[35]

The linewidths (FWHM $=20$–$30\ cm^{-1}$) in the aqueous solution are somewhat larger than those observed in Gd^{3+}:LaF_3 at room temperature. The additional broadening probably results from greater statistical distribution of line centers rather than from homogeneous broadening, since the linewidths of the $^6P_{5/2}$ components shown in Fig. 10 are nearly identical to those observed[30] in the frozen aqueous solution at 4 K. Furthermore, in those instances where lines are sufficiently resolved to permit a meaningful line-shape analysis, we find that our lines fit more closely to a Gaussian than to a Lorentzian profile, although in most cases the shapes appear nevertheless to be intermediate. Most likely, therefore, the homogeneous width is comparable to the room-temperature homogeneous width in crystals. The homogeneous width is determined by collisional perturbation of the hydration complex, which causes both radiationless transitions between optical levels as well as phase perturbation (T_2 mechanism) of the optical state. Since the radiationless transition rates are much smaller than the observed widths, however, the phase interruption mechanism must determine the homogeneous width.

IV. ANALYSIS OF TWO-PHOTON TRANSITION INTENSITIES

A. General theoretical framework

The line strength S_{TPA} of a two-photon transition from a ground state g with components $|f^N\psi JM)$ to an excited state f with components $|f^N\psi'J'M')$ is proportional to

$$\sum_{M,M'} \left| \sum_{n} \Delta_n^{-1} (g \mid \vec{E}\cdot\vec{D} \mid n)(n \mid \vec{E}\cdot\vec{D} \mid f) + \sum_{m,n} \Delta_m^{-1}\Delta_n^{-1} (g \mid \vec{E}\cdot\vec{D} \mid m)(m \mid V \mid n)(n \mid \vec{E}\cdot\vec{D} \mid f) \right.$$
$$\left. + \sum_{l,m,n} \Delta_l^{-1}\Delta_m^{-1}\Delta_n^{-1} (g \mid \vec{E}\cdot\vec{D} \mid l)(l \mid V \mid m)(m \mid V' \mid n)(n \mid \vec{E}\cdot\vec{D} \mid f) + \cdots \right|^2 , \quad (1)$$

where second-, third-, and fourth-order terms in the perturbation series have been shown explicitly. Δ_i is the energy $E_i - h\nu$ of the intermediate state above the single-photon energy, and $\vec{D}$ is the sum of the radius vectors $\vec{r}_j$ for all electrons j. For Gd^{3+} the intermediate states, l, m, and n belong to configurations of the form f^6d, f^6g, and $d^{-1}f^8$ of which $4f^65d$, being lowest in energy, is the most important. Göppert-Mayer[36] developed the theory of two-photon absorption on the basis of the second-order term alone, which proves adequate in the vast majority of cases. The higher-order terms introduce extra energy denominators, as well as interactions V and V' among levels of the intermediate configurations. V and V' represent all or some part of the static Hamiltonian $H = U + H_c + H_{so} + H_{CF}$, where the terms on the right-hand side are central-field, interelectronic Coulomb, spin-orbit, and crystal-field (CF) potentials, respectively. If chosen judiciously, V and V' can overcome angular momentum selection rules which limit the magnitude of the second-order linkage of g to f. With $V = H_{so}$, for example, the spin selection rule $\Delta S = 0$ breaks down in third order. A direct linkage of the ^8S ground state of Gd^{3+} to the sextet excited states thus becomes possible. Similarly, with $V = H_{CF}$, the selection rules $\Delta L, \Delta J \leq 2$ can be overcome in third order. In such cases the higher-order terms can rival or exceed the second-order terms in magnitude despite the extra energy denominator. Eventually, however, the perturbation series converges, since beyond some finite order, no selection rules remain to be overcome for a given transition. The extra energy denominators are then no longer compensated by large numerators at higher orders.

An expression similar to the second-order term in (1) occurs in the theory of single-photon electric dipole absorption for lanthanides,[10,11] where the role of the second photon is replaced by the noncentrosymmetric part of the crystal field. Judd[10] and Ofelt[11] showed that the sum over intermediate states could be evaluated by a closure approximation, in which Δ_n is assumed constant for each excited configuration. Axe,[12] employing the same approximation, showed that the second-order line strength of a two-photon transition could be written as

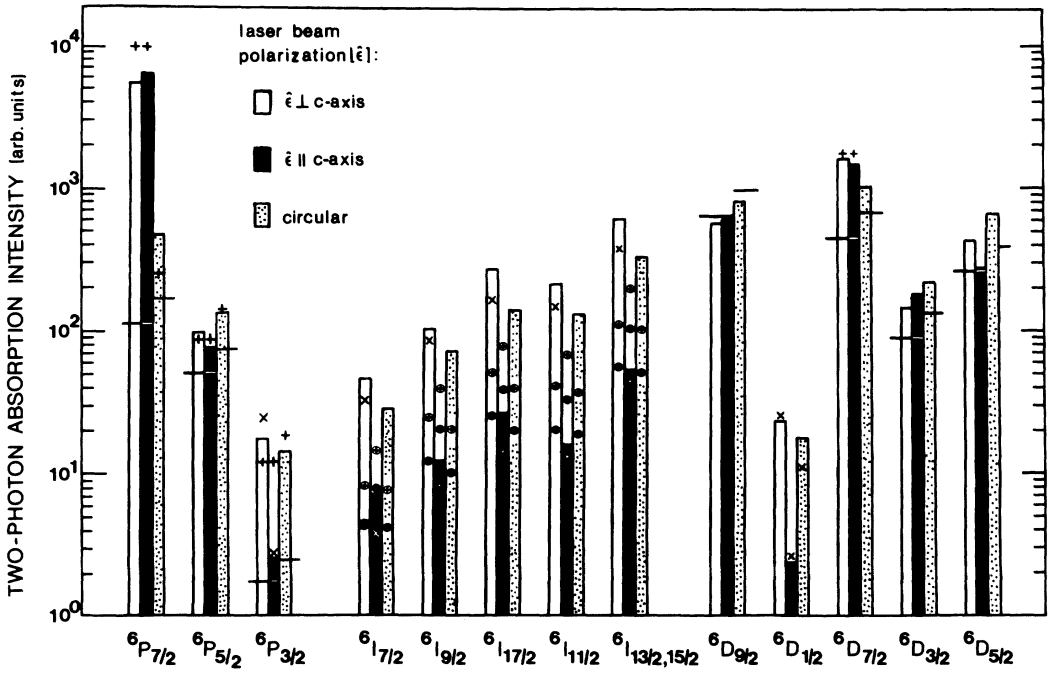

FIG. 12. Relative two-photon absorption line strengths for Gd^{3+}:LaF_3 for the three indicated polarizations of the excitation beam. Horizontal lines denote predictions of the second-order theory. Crosses (+) denote line strengths predicted by including third-order terms in the spin-orbit interaction, closed circles by including third-order terms in the crystal-field interaction, and circled crosses by including fourth-order terms involving both spin-orbit and crystal-field interactions. When J mixing among the $4f^7$ levels is taken into account, the $\times$'s show the predicted intensities for $^6P_{3/2}$, ^6I_J, and $^6D_{1/2}$.

TABLE I. Stark component level positions observed in a 0.5M solution of Gd^{3+} in dilute perchloric acid ($HClO_4$). Stark components were not well resolved for the ^6I levels.

Multiplet	Observed components (cm^{-1})
$^6P_{7/2}$	32 116
	32 138
	32 164
	32 180
$^6P_{5/2}$	32 698
	32 736
	32 759
$^6P_{3/2}$	33 286
	33 329
$^6I_{7/2}$[a]	35 837
	35 866
	35 879
	35 909
$^6D_{9/2}$	39 553
	39 614
	39 639
	39 667
$^6D_{1/2}$	40 510
$^6D_{7/2}$	40 619[b]
	40 678[b]
$^6D_{3/2}$	40 778
	40 822
$^6D_{5/2}$	40 911
	40 947
	40 996

[a]Data for 0.1M perchlorate solution from Svoronos *et al.* (Ref. 29).

[b]Probably comprises two unresolved components.

$$S_{\mathrm{TPA}}=(\tfrac{18}{175})E_{df}^{-2}[(\underline{E}^{(1)}\underline{E}^{(1)})^{(2)}]^2 \times r_{fd}^2(f^7[\psi J]||\underline{U}^{(2)}||f^7[\psi' J'])^2 , \quad (2)$$

where r_{fd} is the radial integral $(f \mid r \mid d)$ and $E_{df}\simeq 10^5$ cm^{-1} is the average energy of $4f^6 5d$ above the single-photon energy $h\nu$. Brackets around the term designation denote intermediate coupling wave functions. Expression (2) can also be derived using second-quantization techniques.[9] To express the intensity of individual Stark components, we must forego the sum over M' values used in deriving (2).

Several important points about the result (2) can be made. Firstly, since only a single term occurs, the *ratio* of the intensities of two transitions is given simply by the ratios of the squares of the second-rank reduced matrix elements $(f^7\psi J||\underline{U}^{(2)}||f^7\psi' J')^2$ for the two transitions. These quantities depend only on the angular parts of the wave functions, which are known with great precision from energy-level analysis, and accurate tables[14] in the full intermediate coupling approximation are readily available. Secondly, when both photons have the same linear polarization, the polarization-dependent factor $[(\underline{E}^{(1)}\underline{E}^{(1)})^{(2)}]^2$ is equal to $\frac{2}{3}E^4$ for any polarization direction. This isotropy is a consequence of the free-ion nature of the description of TPA in second order. Thirdly, other polarization combinations lead to different, though readily predicted, line strengths. For two equivalently circularly polarized photons, for example, $[(\underline{E}^{(1)}\underline{E}^{(1)})^{(2)}]^2$ equals $(1111 \mid 1122)E^4=E^4$, yielding a 50% greater line strength than for linear polarization. The above predictions require no phenomenological parameters, as do analogous predictions in the theory of one-photon oscillator strengths.[10,11] Measurements of the relative line strengths of different transitions and the polarization dependence of each transition thus provide rigorous tests of the second-order theory, as do measurements of the polarization dependence of individual Stark components.

Axe's second-order theory satisfactorily explained the relative intensities of electronic Raman transitions in Pr^{3+},[37] the only relevant data available at the time of its formulation. Its failure to explain most of the TPA data for Gd^{3+} in Fig. 12, however, prompts reexamination of the underlying assumptions. Term dependence of the radial integral r_{fd}, which has been assumed constant, would be far too modest to explain discrepancies of the magnitude shown. The closure approximation could be questioned, but the widespread success of the theory of single-photon oscillator strengths argues strongly in favor of its validity.

In the following discussion, therefore, we introduce the third- and fourth-order terms in (1) into the analysis. The closure approximation is again employed, leaving compound operators acting between levels of $4f^7$. These operators must be recoupled to convert them to simpler standard operators for which matrix elements can be readily computed. Second-quantization techniques[9,38] prove especially powerful in performing the required manipulations. Full derivation of the higher-order operators (see Ref. 8) are planned to be reserved for a later publication. For now, the fully recoupled operators will be stated and used in analyzing the Gd^{3+}:LaF_3 data. Insofar as integrated intensities or line strengths are concerned, the analysis applies also to the aqueous solution data. No attempt will be made, however, to analyze the Stark-component intensities of the solution sample, since the level assignments are not known and since data obtained with a single excitation beam do not sufficiently characterize the excited-state symmetries in a sample of randomly oriented ions.[35]

B. $^8S_{7/2}\rightarrow {}^6P_{5/2},{}^6D_{9/2,3/2,5/2}$: Second-order terms

Since the second-order expression (2) evidently explains the integrated intensities of $^8S_{7/2}\rightarrow {}^6P_{5/2},{}^6D_{9/2,3/2,5/2}$, we now compare the experimental Stark-component intensities of these four transitions in Gd^{3+}:LaF_3 with second-order predictions. Since the ground-state splitting is not resolved in Gd^{3+}, all components of the ground state contribute to the intensity of each observed Stark component. We therefore retain the sum over M, but compute the in-

tensity for each value of M' separately. The intensity of the component $|f^7\psi' J' M'\rangle$ is then proportional to

$$\sum_M \left| \frac{1}{2}\begin{pmatrix} J' & \frac{7}{2} & 2 \\ M' & -M & -2 \end{pmatrix} + \left(\frac{1}{6}\right)^{1/2}\begin{pmatrix} J' & \frac{7}{2} & 2 \\ M' & -M & 0 \end{pmatrix} + \frac{1}{2}\begin{pmatrix} J' & \frac{7}{2} & 2 \\ M' & -M & 2 \end{pmatrix}\right|^2 \quad \text{for } \vec{E}\perp\hat{z}\,, \tag{3a}$$

$$\sum_M \frac{2}{3}\begin{pmatrix} J' & \frac{7}{2} & 2 \\ M' & -M & 0 \end{pmatrix}^2 \quad \text{for } \vec{E}\|\hat{z}\,, \tag{3b}$$

and

$$\sum_M \begin{pmatrix} J' & \frac{7}{2} & 2 \\ M' & -M & 2 \end{pmatrix}^2 \tag{3c}$$

for circular polarization. Expressions (3) result from substituting the appropriate spherical tensor form of the electric field vectors for each polarization into the TPA operator $(\underline{E}^{(1)}\underline{E}^{(1)})^{(2)}\cdot\underline{U}^{(2)}$ and dropping common numerical factors.

For the approximately D_{3h} substitution site symmetry, the crystal-field operator may be written

$$H_{\mathrm{CF}} = \sum_n [B_0^{(2)}C_0^{(2)} + B_0^{(4)}C_0^{(4)} + B_0^{(6)}C_0^{(6)} + B_6^{(6)}(C_6^{(6)} + C_{-6}^{(6)})]_n\,, \tag{4}$$

where the $C_q^{(k)}$ are modified spherical harmonic operators $[4\pi/(2k+1)]^{1/2}Y_{kq}$, and $B_q^{(k)}$ are coefficients determined by the charge distribution of the surrounding lattice and by radial integrals of the f^7 electrons. From (4) we conclude that for $J \le \frac{5}{2}$, M' is rigorously a good quantum number, and the results (3) may be applied without alteration to compute Stark-component intensities. For $J > \frac{5}{2}$, the $B_6^{(6)}$ terms mix M' values to a small extent. In these cases, the appropriate eigenfunctions with mixed azimuthal quantum numbers must be used in conjunction with expressions (3) to derive Stark-component intensities.

The results of such computations for $^8S_{7/2} \rightarrow {}^6P_{5/2}, {}^6D_{9/2,3/2,5/2}$ are compared with experimental data in Figs. 2 and 3. For $^6P_{5/2}$ and $^6D_{5/2}$, a satisfying account of the Stark-component intensities for all three polarizations is obtained with the M' values shown at the base of Fig. 2. The discrepancy for $^6D_{5/2}$ for $\vec{E}\|\hat{z}$ is less than it appears at first sight, since the lowest-energy component is broader than the other two. Crystal-field calculations[14,22] alone have not assigned the M' values for these two multiplets unambiguously. For $^6P_{5/2}$, the calculations of Carnall *et al.*[14] yield nearly identical energy values for the two lowest-energy components $M' = \pm\frac{3}{2}$ and $\pm\frac{5}{2}$, while for $^6D_{5/2}$, the calculated positions of the two highest-energy components $M' = \pm\frac{5}{2}$ and $\pm\frac{1}{2}$ are nearly the same, even though the observed components are well separated in both cases. From this information alone, therefore, one cannot decide which M' value belongs to which observed component. The calculated two-photon intensities shown in Fig. 2, however, demonstrate convincingly that the uncertain assignments must be as shown.

For $^6D_{3/2}$, no reproducible variation in the Stark-component intensities with polarization was observed apart from the expected 50% strengthening of the integrated multiplet intensity for circular polarization, although no strong variation is predicted either. J admixtures of the nearby $^6D_{7/2,5/2}$ levels probably account for the failure of the modest predicted contrast between the two linear polarizations to show.

$^6D_{9/2}$, on the other hand, is well separated from neighboring multiplets, so that J mixing can be neglected. Nevertheless, for $\vec{E}\|\hat{z}$, the expected drop in the intensities of the $M' = \pm\frac{9}{2}$ and $\pm\frac{1}{2}$ components and the corresponding strengthening of the remaining components is not observed, although curiously the agreement is quite good for the other polarizations. Here M' refers to the principal component of the eigenfunctions. No reassignment of the M' values, which are taken from crystal-field calculations,[14] improves the agreement, and the good agreement between observed and calculated crystal-field splittings[14] suggests that the M' values have been correctly assigned. The higher-order contributions discussed below prove to be negligible for $^6D_{9/2}$ and thus cannot remedy the situation.

Possibly $^6D_{9/2}$ is particularly sensitive to the distortion of D_{3h} to a lower symmetry, in which new off-diagonal elements enter the crystal-field matrix, causing greater mixing of M' values. The ESR results of Jones *et al.*[15] for 0.01 mol.% Gd^{3+}:LaF_3 have indicated that the crystal-field terms proportional to $B_2^{(4)}$ and $B_4^{(4)}$ are important. Since $([^6D_{9/2}]\|\underline{U}^{(4)}\|[^6D_{9/2}])$ is quite large,[14] these crystal-field terms can cause substantial admixtures of other M' values into $M' = \pm\frac{9}{2}, \pm\frac{1}{2}$, thus potentially explaining their observed intensities. Since $([^6P_{5/2}]\|\underline{U}^{(4)}\|[^6P_{5/2}])$ is very small[14] and $([^6D_{3/2}]\|\underline{U}^{(4)}\|[^6D_{3/2}])$ is zero, $^6P_{5/2}$ and $^6D_{3/2}$ would be unaffected by these new crystal-field terms, although $^6D_{5/2}$ would be affected. This result indicates the need for a closer examination of the effect of the distortion from D_{3h} upon the energy levels and eigenfunctions of Gd^{3+}:LaF_3, to see whether a consistent account of the Stark-component intensities of $^6D_{9/2,5/2}$, on the one hand, and the crystal-field splittings of all levels, on the other hand, emerges.

C. $^8S_{7/2} \rightarrow {}^6P_{7/2,3/2}, {}^6D_{7/2,1/2}$: Third-order terms in the spin-orbit interaction

Judd and Pooler[9] introduced the third-order terms with $V = H_{so}$ and found that the anomalous line strength observed[6] for $^8S_{7/2} \rightarrow {}^6P_{7/2}$ could be explained. We now expand this third-order analysis to all observed line strengths of Gd^{3+}:LaF_3 and show in addition that the Stark-component intensities of $^6P_{7/2}$, $^6D_{7/2}$, and $^6D_{1/2}$, as well as the strong anisotropy of $^6P_{3/2}$, can be explained in quantitative detail when, and only when, third-order terms with $V = H_{so}$ are taken into account.

Judd and Pooler[9] showed that following double closure over intermediate states of the $4f^6 5d$ configuration and a lengthy process of operator recoupling, the third-order operator which acts between f^7 $^8S_{7/2}$ and the various excited states of Gd^{3+} could be recast in the form

$$-(42)^{1/2}\zeta_f/E_{df}^2\underline{E}^{(1)}\cdot\underline{E}^{(1)}\underline{W}^{(11)0}+6(\tfrac{3}{2})^{1/2}E_{df}^{-2}\sum_{t,\lambda}(-1)^{\lambda+1}(2\lambda+1)^{1/2}$$

$$\times\left[(7)^{1/2}\begin{Bmatrix}t&3&3\\3&1&3\end{Bmatrix}\begin{Bmatrix}2&1&3\\t&3&1\end{Bmatrix}\zeta_f+(\tfrac{5}{2})^{1/2}\begin{Bmatrix}1&3&2\\1&3&2\\t&\lambda&1\end{Bmatrix}\zeta_d\right](\underline{E}^{(1)}\underline{E}^{(1)})^{(t)}\cdot\underline{W}^{(1\lambda)t}\,, \tag{5a}$$

where ζ_f and ζ_d are the spin-orbit coupling constants for f and d electron, respectively, and $\underline{W}^{(ij)k}$ represents a sum $\sum_n[\underline{w}^{(ij)k}]_n$ of single-particle double-tensor operators[39] with rank i in spin space, rank j in orbital space, and magnitude defined by

$$(nl||\underline{w}^{(ij)}||n'l')=\delta(n,n')\delta(l,l')(2i+1)^{1/2}(2j+1)^{1/2}\,.$$

The spin and orbital parts are coupled to rank k in the space of total angular momentum. In (5a) the term with $t=1$ vanishes for our present application, since with a single excitation source the electric field vectors are identical, so that $(\underline{E}^{(1)}\underline{E}^{(1)})^{(1)}$ represents a cross product of identical vectors. Terms with $t=0,2$, however, can be nonvanishing.

The relative importance of the various terms $\underline{W}^{(1\lambda)t}$ depends on the particular two-photon transition being investigated. For ${}^8S\rightarrow{}^6P$, terms with $\lambda=1$ dominate since they directly link $L=0$ to $L=1$. The remaining terms in (5a) can therefore be discarded when considering these transitions. Similarly, for ${}^8S\rightarrow{}^6D$, terms with $\lambda=2$ dominate. There are no terms in (5a), however, which can directly link ${}^8S$ to ${}^6I$, since λ can be at most 3. We now examine the third-order contribution to the ${}^6P$ and ${}^6D$ lines in more detail.

1. ${}^8S_{7/2}\rightarrow{}^6P_J$

For ${}^8S\rightarrow{}^6P$, the relevant part of the operator (5a) is[40]

$$-2(\tfrac{2}{21})^{1/2}E_{df}^{-2}(9\zeta_f+\zeta_d)\underline{E}^{(1)}\cdot\underline{E}^{(1)}\underline{W}^{(11)0}$$
$$+2(\tfrac{1}{1400})^{1/2}E_{df}^{-2}(9\zeta_f-4\zeta_d)(\underline{E}^{(1)}\underline{E}^{(1)})^{(2)}\cdot\underline{W}^{(11)2}\,. \tag{5b}$$

The first term is rank zero and thus contributes only to ${}^6P_{7/2}$, whereas the second term is rank 2 and contributes to all three ${}^6P$ transitions. Furthermore, the first term vanishes for circular polarization since $\underline{E}^{(1)}\cdot\underline{E}^{(1)}=0$ and has the same nonzero value for any linear polarization. This scalar term thus has all the necessary features to explain the enormous isotropic enhancement of ${}^8S_{7/2}\rightarrow{}^6P_{7/2}$ for linear polarization.

To compute the line strengths quantitatively, the operator (5b) must first be added to the second-order operator before the square modulus of the matrix element is taken. Taking $\vec{E}||\hat{z}$, we then find the line strength of ${}^8S_{7/2}\rightarrow{}^6P_J$ to be

$$S=\tfrac{4}{21}E^4E_{df}^{-2}\sum_{MM'}\left|-\tfrac{3}{5}(5)^{1/2}\begin{pmatrix}J&\frac{7}{2}&2\\M'&-M&0\end{pmatrix}([{}^8S_{7/2}]||\underline{U}^{(2)}||[{}^6P_J])\right.$$
$$-\tfrac{1}{10}(9\zeta_f-4\zeta_d)E_{df}^{-1}\begin{pmatrix}J&\frac{7}{2}&2\\M'&-M&0\end{pmatrix}({}^8S_{7/2}||\underline{W}^{(11)2}||{}^6P_J)$$
$$\left.+(2)^{1/2}(9\zeta_f+\zeta_d)E_{df}^{-1}\begin{pmatrix}J&\frac{7}{2}&0\\M'&-M&0\end{pmatrix}({}^8S_{7/2}||\underline{W}^{(11)0}||{}^6P_J)\right|^2. \tag{5c}$$

Analogous expressions are obtained for $\vec{E}\perp\hat{z}$ and circular polarization. For ${}^6P_{7/2}$, circular polarization, and ${}^6P_{5/2,3/2}$, all polarizations, the scalar term vanishes. The sum over M and M' is quickly evaluated by using the orthogonality relation for 3-j symbols (Edmonds[41] Eq. 3.7.8). A cross term between the two second-rank terms arises. The values of the reduced matrix elements are shown in Table II. Using the numerical values $\zeta_f=2\zeta_d=1500$ cm^{-1} and $E_{df}=150000$ cm^{-1}, we find that the ratios of the third-order to the second-order contributions are

${}^6P_{7/2}$ linear: 105 circular: 0.45,

${}^6P_{5/2}$ all E: 1.0,

${}^6P_{3/2}$ all E: 10.

The third-order scalar term indeed causes the enormous enhancement of ${}^6P_{7/2}$ for linear polarization, while the third-order second-rank term increases the intensities of ${}^6P_{5/2,3/2}$ by lesser and unequal amounts without altering the polarization dependence predicted in second order. The calculated relative line strengths are shown by crosses (+) in Fig. 12, and agree very well with the data for ${}^6P_{7/2,5/2}$. The strong anisotropy of ${}^6P_{3/2}$, however, remains unexplained, a point to which we return shortly.

We obtain predictions of the Stark-component intensities of the ${}^6P_J$ multiplets by evaluating (5c) for each value of M' rather than summing. For ${}^6P_{5/2}$, the third-order operator proportional to $(\underline{E}^{(1)}\underline{E}^{(1)})^{(2)}\cdot\underline{W}^{(11)2}$ is present in addition to the second-order operator. Since the two operators are of equal rank and depend in the same way on polarization, the analysis of ${}^6P_{5/2}$ in the preceding sec-

TABLE II. Reduced matrix elements for Gd^{3+} which arise in third- and fourth-order contributions to two-photon absorption involving the spin-orbit interaction among the intermediate states. Brackets around a term designation indicate that spin-orbit admixtures into the L-S—coupled state have been taken into account. E_{DP} (E_{PS}) denotes the average energy separation of the ^6P states from the ^6D (^8S) states.

Transitions	Reduced matrix elements of $W^{(1\lambda)t}$
$^8S \rightarrow {}^6P$	$(^8S_{7/2}\|\|\underline{W}^{(11)0}\|\|^6P_{7/2}) = +(\frac{8}{3})^{1/2}$
	$(^8S_{7/2}\|\|\underline{W}^{(11)2}\|\|^6P_{7/2}) = +(\frac{20}{7})^{1/2}$
	$(^8S_{7/2}\|\|\underline{W}^{(11)2}\|\|^6P_{5/2}) = -6(\frac{1}{7})^{1/2}$
	$(^8S_{7/2}\|\|\underline{W}^{(11)2}\|\|^6P_{3/2}) = +4(\frac{1}{3})^{1/2}$
$^8S \rightarrow {}^6I$	$(^8S_{7/2}\|\|\underline{W}^{(16)5,6}\|\|^6I_{7/2}) = -2(\frac{1}{39})^{1/2}, -2(\frac{1}{3})^{1/2}$
	$(^8S_{7/2}\|\|\underline{W}^{(16)5,6}\|\|^6I_{9/2}) = +2(\frac{5}{39})^{1/2}, +\frac{10}{7}(\frac{5}{3})^{1/2}$
	$(^8S_{7/2}\|\|\underline{W}^{(16)5,6}\|\|^6I_{11/2}) = -12(\frac{1}{65})^{1/2}, -\frac{12}{7}(2)^{1/2}$
	$(^8S_{7/2}\|\|\underline{W}^{(16)5,6}\|\|^6I_{13/2}) = +5(\frac{2}{13})^{1/2}, +\frac{1}{7}(\frac{1190}{3})^{1/2}$
	$(^8S_{7/2}\|\|\underline{W}^{(16)5,6}\|\|^6I_{15/2}) = -\frac{10}{3}(\frac{22}{91})^{1/2}, -\frac{2}{7}(110)^{1/2}$
$^8S \rightarrow {}^6D$	$(^8S_{7/2}\|\|\underline{W}^{(12)2}\|\|^6D_{9/2}) = +(\frac{11}{105})^{1/2}$
	$(^8S_{7/2}\|\|\underline{W}^{(12)2}\|\|^6D_{7/2}) = -\frac{1}{2}(\frac{10}{21})^{1/2}$
	$([^8S_{7/2}]\|\|\underline{W}^{(11)0}\|\|[^6D_{7/2}]) = (\frac{6}{5})^{1/2}\zeta_f(+3E_{DP}^{-1} - E_{PS}^{-1})$
	$(^8S_{7/2}\|\|\underline{W}^{(12)2}\|\|^6D_{5/2}) = +(\frac{3}{35})^{1/2}$
	$(^8S_{7/2}\|\|\underline{W}^{(12)2}\|\|^6D_{3/2}) = -\frac{2}{7}(2)^{1/2}$

tion remains valid. The third-order operator simply increases the predicted Stark-component intensities uniformly by about a factor of 2 without altering the relative intensities or polarization dependence.

For $^6P_{7/2}$, however, the third-order scalar operator is present in addition to the two second-rank operators. Matrix elements of the scalar operator interfere with those of the second-rank operators, the type and degree of interference depending on the value of M' and the polarization. Explicit calculation shows that for $\vec{E}\|\hat{z}$, the three matrix elements interfere constructively for $M' = \pm\frac{1}{2}$ and $\pm\frac{3}{2}$, resulting in larger intensities, while they interfere destructively for $M' = \pm\frac{5}{2}$ and $\pm\frac{7}{2}$, resulting in smaller intensities. For $\vec{E}\perp\hat{z}$, exactly the reverse is true. For circular polarization, the scalar term vanishes. Full numerical details are given in Ref. 8. The results of these computations are compared with the experimental Stark-component intensities in Fig. 4 and show excellent agreement with the data. In making this comparison, the 50% greater width of the highest-energy component, which results from phonon-induced relaxation to the lower components, must be taken into account. The slight mixing of the $M' = \pm\frac{7}{2}$ and $\pm\frac{5}{2}$ values by the D_{3h} crystal field has been included in arriving at the theoretical values shown. The M' values shown at the base of Fig. 4 agree with those obtained by crystal-field calculations.[14,22]

The strong anisotropy of $^6P_{3/2}$, as with any anisotropy, must involve the crystal field in some capacity. In the present case, its role is to mix a small percentage of $^6P_{7/2}$ into $^6P_{3/2}$. The two components $M' = \pm\frac{1}{2}, \pm\frac{3}{2}$ are then written

$$|\{^6P_{3/2}, M'\}\rangle = |[^6P_{3/2}, M']\rangle + \epsilon_{M'M''}|\,^6P_{7/2}, M''\rangle ,$$

where the curly brackets around the term designation indicate that J mixing has been taken into account. For the D_{3h} crystal field (4), only admixtures for which $M' = M''$ are present, so we write the coefficient simply as $\epsilon_{M'}$. Contributions to the intensity of $^6P_{3/2}, M'$ now come not only from the matrix elements of the second- and third-order second-rank operators, which for brevity we write as $\underline{Q}^{(2)}(2)$ and $\underline{Q}^{(2)}(3)$, respectively, but from matrix elements of the third-order scalar operator $\underline{Q}^{(0)}(3)$ which acts only upon the $^6P_{7/2}$ admixture. The effect of this last matrix element is to interfere destructively with the other two for $\vec{E}\|\hat{z}$, and constructively for $\vec{E}\perp\hat{z}$, creating the strong observed anisotropy.

To demonstate this interference quantitatively, numerical values of the three matrix elements involved are listed in Table III for the polarizations studied. For $\vec{E}\|\hat{z}$, all three operators have lower index $q = 0$ and thus interfere with one another. For each M', this trio of matrix elements, listed on a single row in Table III, must be added before the sum is squared. For $\vec{E}\perp\hat{z}$, $\underline{Q}^{(0)}(3)$ remains unchanged apart from a sign change, but the two second-rank operators now become sums of three tensor operators of the form

$$(\tfrac{1}{2})O_2^{(2)} + (\tfrac{1}{6})^{1/2}O_0^{(2)} + (\tfrac{1}{2})O_{-2}^{(2)} ,$$

of which only the middle one interferes with scalar opera-

TABLE III. Matrix elements of second- and third-order two-photon absorption operators between components of the ground state $[^8S_{7/2},M]$ and components of the excited state $[^6P_{3/2},M']$. $\epsilon_{M'}$ is the coefficient of $[^6P_{7/2},M']$ which is admixed into $[^6P_{3/2},M']$. The common factor $-2E^2/E_{df}$ has been dropped from all matrix elements. In determining the intensity of the component M', matrix elements appearing on the same row must be added before squaring.

Polarization	M,M'	$[\underline{Q}^{(2)}(2)]_{MM'}$[a]	$[\underline{Q}^{(2)}(3)]_{MM'}$[b]	$[\underline{Q}^{(0)}(3)]_{MM'}$[c]
$\vec{E}\perp\hat{z}$	$\mp\frac{3}{2},\pm\frac{1}{2}$	-0.000096	-0.0207[d]	0
	$\pm\frac{1}{2},\pm\frac{1}{2}$	-0.00015	-0.0324[d]	$-1.78\epsilon_{1/2}$[d]
	$\pm\frac{5}{2},\pm\frac{1}{2}$	-0.00017	-0.0357[d]	0
	$\mp\frac{1}{2},\pm\frac{3}{2}$	-0.000043	-0.0092[d]	0
	$\pm\frac{3}{2},\pm\frac{3}{2}$	-0.00011	-0.0238[d]	$-1.78\epsilon_{3/2}$[d]
	$\pm\frac{7}{2},\pm\frac{3}{2}$	-0.00025	-0.0546[d]	0
$\vec{E}\|\|\hat{z}$	$\pm\frac{1}{2},\pm\frac{1}{2}$	-0.00030	-0.0639[d]	$+1.78\epsilon_{1/2}$[d]
	$\pm\frac{3}{2},\pm\frac{3}{2}$	-0.00022	-0.0476[d]	$+1.78\epsilon_{3/2}$[d]
Circular	$+\frac{5}{2},+\frac{1}{2}$	-0.00033	-0.0714[d]	0
	$+\frac{3}{2},-\frac{1}{2}$	-0.00019	-0.0412[d]	0
	$+\frac{7}{2},+\frac{3}{2}$	-0.00051	-0.1091[d]	0
	$+\frac{1}{2},-\frac{3}{2}$	-0.000085	-0.0184[d]	0

[a] $\underline{Q}^{(2)}(2)=-\frac{3}{5}(\frac{5}{14})^{1/2}(\underline{E}^{(1)}\underline{E}^{(1)})^{(2)}\cdot\underline{U}^{(2)}$.

[b] $\underline{Q}^{(2)}(3)=-\frac{1}{2}(\frac{1}{14})^{1/2}(\zeta/E_{df})(\underline{E}^{(1)}\underline{E}^{(1)})^{(2)}\cdot\underline{W}^{(11)2}$.

[c] $\underline{Q}^{(0)}(3)=-10(\frac{2}{7})^{1/2}(\zeta/E_{df})(\underline{E}^{(1)}\underline{E}^{(1)})^{(0)}\cdot\underline{W}^{(11)0}$.

[d] Multiply by $\zeta/E_{df}\simeq 0.01$ to obtain the value of the matrix element.

tor. For each M', therefore, the matrix elements of $(\frac{1}{6})^{1/2}O_0^{(2)}$ and $(\frac{1}{6})^{1/2}O_0^{(2)}(3)$ are added to the matrix element of $O_0^{(0)}(3)$ before squaring, and this result is then added to the squares of the matrix elements of $(\frac{1}{2})[O_{\pm 2}^{(2)}(2)+O_{\pm 2}^{(2)}(3)]$ to obtain the intensity of the component M'. Finally, for circular polarization the scalar operator vanishes.

Table III shows that for $\vec{E}\|\hat{z}$, the matrix element of $O_0^{(0)}(3)$ exactly cancels the sum of the other two matrix elements if $\epsilon_{M'}$ is *positive* and equal to about 0.05 for $M'=\pm\frac{1}{2}$ and 0.04 for $M'=\pm\frac{3}{2}$. Using first-order perturbation theory, we find that

$$\epsilon_{M'}^{(1)}=\begin{cases} E_{3/2,7/2}^{-1}([^6P_{7/2},M']\,|\,H_{\rm CF}\,|\,[^6P_{3/2},M']) \\ +0.007 \quad \text{for } M'=\pm\frac{1}{2} \\ +0.005 \quad \text{for } M'=\pm\frac{3}{2}\ . \end{cases}$$

The numerical results were obtained using[14] $E_{3/2,7/2}=1000\ \text{cm}^{-1}$, $B_0^{(2)}=210\ \text{cm}^{-1}$. The signs are indeed positive, but the magnitude is too small to produce the strong observed anisotropy. We find, however, that second-order linkages of the form

$$\epsilon_{M'}^{(2)}=E_{3/2,7/2}^{-1}\times\sum_i E_i^{-1}(^6P_{7/2},M'\,|\,H_{\rm CF}\,|\,i)(i\,|\,H_{\rm CF}\,|\,^6P_{3/2},M')\ ,$$

particularly those for which i is ^6I_J, are much more important in this case. Explicit evaluation of the second-order coefficient using $i=^6I_J$ and a constant energy separation $E_{IP}=4000\ \text{cm}^{-1}$ of ^6I from ^6P yields the results

$$\epsilon_{1/2}^{(2)}=\tfrac{20}{169}(\tfrac{10}{7})^{1/2}E_{3/2,7/2}^{-1}E_{IP}^{-1}[\tfrac{7}{22}(B_0^{(6)})^2+(B_6^{(6)})^2]$$
$$=+0.030\ ,$$
$$\epsilon_{3/2}^{(2)}=\frac{2500}{3\times 7\times 13^2}(\tfrac{7}{2})^{1/2}E_{3/2,7/2}^{-1}\times E_{IP}^{-1}[\tfrac{127}{275}(B_0^{(6)})^2+(B_6^{(6)})^2]$$
$$=+0.026\ ,$$

where the values [14] $B_0^{(6)}=1250\ \text{cm}^{-1}$ and $B_6^{(6)}=600\ \text{cm}^{-1}$ have been used. The total admixtures are then

$$\epsilon_{1/2}=\epsilon_{1/2}^{(1)}+\epsilon_{1/2}^{(2)}=+0.037\ ,$$
$$\epsilon_{3/2}=\epsilon_{3/2}^{(1)}+\epsilon_{3/2}^{(2)}=+0.031\ ,$$

which are now quite close to the values required for cancellation for $\vec{E}\|\hat{z}$. In fact, the data are best fit with the values $\epsilon_{1/2}=+0.032$ and $\epsilon_{3/2}=+0.028$ when $\zeta_f=0.01E_{df}$. The result of choosing these values is shown by the closed circles in Fig. 5 and by the $\times$'s on the bar graph in Fig. 12. By contrast, the horizontal lines in Fig. 5 show the isotropic intensities predicted when the

$^6P_{7/2}$ admixture is neglected. Every detail of the experimental $^6P_{3/2}$ scan is now correctly explained.

2. $^8S_{7/2} \rightarrow {}^6D_J$

The relevant part of the third-order operator (5a) for the ^6D lines is

$$+\tfrac{3}{5}(\tfrac{3}{14})^{1/2}(\zeta_f/E_{df}^2)(\underline{E}^{(1)}\underline{E}^{(1)})^{(2)}\cdot\underline{W}^{(12)2} . \quad (5d)$$

The term proportional to ζ_d vanishes exactly, while the scalar term does not contribute in the Russell-Saunders limit. Using the matrix elements from Table II, we find that the ratios of the third-order to second-order contributions for all polarizations are

$$^6D_{9/2}{:}0.032 , \; ^6D_{7/2}{:}0.041 ,$$

$$^6D_{5/2}{:}0.045, \; ^6D_{3/2}{:}0.105 , \; ^6D_{1/2}{:}0 .$$

In all cases the third-order term contributes only a few percent to the line strength. The account given previously of the $^6D_{9/2,3/2,5/2}$ intensities in terms of the second-order theory alone is, therefore, fully justified.

One other third-order contribution to the ^6D lines must, however, be considered. Since the coefficient of the scalar operator $\underline{W}^{(11)0}$ in (5b) is over 20 times larger than the coefficient of the second-rank operator in (5d), it has the potential to contribute significantly to $^8S_{7/2} \rightarrow {}^6D_{7/2}$ in the intermediate coupling approximation, even though it cannot directly link the major components of the ground- and excited-state wave functions. The value of the matrix element $([^8S_{7/2}]||\underline{W}^{(11)0}||[^6D_{7/2}])$ near the Russell-Saunders limit has therefore been entered in Table II, where the first-order spin-orbit admixtures of ^6P into ^8S and ^6D have been taken into account. The line strength of $^6D_{7/2}$ then contains two significant contributions:

$$\tfrac{4}{21}(E^4/E_{df}^2)\{\tfrac{9}{25}([^8S_{7/2}]||\underline{U}^{(2)}||[^6D_{7/2}])^2 + 2[(9\zeta_f+\zeta_d)^2/E_{df}^2] \times([^8S_{7/2}]||\underline{W}^{(11)0}||[^6D_{7/2}])^2\} .$$

Using $E_{DP}=8500$ cm^{-1}, $E_{PS}=30\,000$ cm^{-1}, and $\zeta_f=2\zeta_d=0.01E_{df}$, we find the ratio of the third-order to the second-order contribution to be about 3.5 for linear polarization, which agrees very well with the data in Fig. 12.

The importance of including the third-order scalar term becomes more evident in analyzing the Stark-component intensities of $^6D_{7/2}$ and $^6D_{1/2}$. For $^6D_{7/2}$ the analysis closely follows that for $^6P_{7/2}$, although the degree of interference is greater since the two contributing terms now have about the same magnitude. Numerical details are presented in Ref. 8. For $\vec{E}||\hat{z}$, destructive interference occurs for $M'=\pm\frac{1}{2}$ and $\pm\frac{3}{2}$ and constructuve interference for $M'=\pm\frac{5}{2}$ and $\pm\frac{7}{2}$; for $\vec{E}\perp\hat{z}$, the reverse occurs. The resulting predictions of Stark-component intensities for $^6D_{7/2}$ are shown by the closed circles in Fig. 6(b), and agree very well with the observed intensities. The vertical bars, by contrast, show the intensities predicted by the second-order term alone. For $M'=\pm\frac{1}{2}$, destructive interference is nearly total for $\vec{E}||\hat{z}$.

An important advantage of the above analysis is its ability to explain quantitatively the strong anisotropy of the neighboring $^6D_{1/2}$ line, shown in Fig. 6(a). $^6D_{1/2}$ contains a small first-order admixture of the $M'=\pm\frac{1}{2}$ component of $^6D_{7/2}$, which is entirely responsible for its intensity,

$$|\{^6D_{1/2},\pm\tfrac{1}{2}\}\rangle = 0.94\,|[^6D_{1/2},\pm\tfrac{1}{2}]\rangle + 0.23\,|[^6D_{7/2},\pm\tfrac{1}{2}]\rangle .$$

$^6D_{1/2}$ is therefore simply a replica of the $M'=\pm\frac{1}{2}$ component of $^6D_{7/2}$, which is an order of magnitude weaker for $\vec{E}||\hat{z}$ than for $\vec{E}\perp\hat{z}$. With the use of second-order theory alone, however, such a strong anisotropy cannot be explained, as shown by the vertical bars in Fig. 6(a).

In the above analysis, the M' assignments for $^6D_{7/2}$ shown in Fig. 6(b) differ from those extracted from crystal-field calculations by Carnall *et al.*[14], where from lowest to highest energy they are $\pm\frac{5}{2}$, $\pm\frac{3}{2}$, $\pm\frac{1}{2}$, and $\pm\frac{7}{2}$. We note, however, that the crystal-field splitting of $^6D_{7/2}$ is exceedingly small compared to other levels of Gd^{3+}:LaF_3, and correspondingly sensitive to parameter choice. A reduction in the importance of the fourth-rank crystal-field terms and/or an increase in the second-rank terms could lead to the ordering of M' values shown in Fig. 6(b). Introducing lower-symmetry components would also change the ordering predicted by Carnall *et al.*[14] Whatever the reason for the discrepancy, we can say with certainty that a totally consistent interpretation of the TPA intensities of $^6D_{7/2}$ and $^6D_{1/2}$ can be obtained if, and only if, the M' values are assigned as in Fig. 6. We therefore propose that these M' assignments are the correct ones.

D. $^8S_{7/2} \rightarrow {}^6I_J$: Third-order terms in the crystal-field interaction and fourth-order terms

Downer *et al.*[7] introduced third-order terms with $V=H_{CF}$ and found that most of the anomalous strength of the six ^6I_J lines and their intensities relative to one another could be explained, although their unusual anisotropy was not explained. Such third-order terms allow $\Delta L, \Delta J \leq 6$, although the spin selection rule $\Delta S=0$ remains in effect. Hence these terms overcome only two of the three angular momentum selection rules which apply to transitions such as $^8S_{7/2} \rightarrow {}^6I_{13/2,15/2,17/2}$. In this section we show that a complete account of the $^8S_{7/2} \rightarrow {}^6I_J$ transitions must include not only third-order terms with $V=H_{CF}$, but fourth-order terms with $V=H_{CF}$ and $V'=H_{so}$ and third-order terms with $V=H_{so}$, the last acting upon a $^6P_{7/2}$ admixture in the ^6I_J wave functions. Second-order contributions are negligible for all of the ^6I_J lines.

Crystal-field splittings within the $4f^{N-1}rd$ configurations are on the order of 10 000 cm^{-1}, an order of magnitude larger than spin-orbit interactions and 2 orders of magnitude larger than crystal-field splittings of $4f^N$ levels. In Ce^{3+}:LaF_3 a total splitting of 15 000 cm^{-1} is observed.[42] In order to parametrize the splitting, we may regard $4f^6 5d$ in the lowest-order approximation as a $4f^6$ core augmented by an isolated $5d$ electron. The enormous crystal-field splittings in the $4f^5 5d$ configuration can then

be interpreted as the action of the crystal field on the $5d$ electron alone. The hexagonal field (4) of LaF_3 splits the ^2D level of the $5d$ electron into three levels, with a total splitting of

$$\tfrac{10}{21}B_0^{(4)}[1+\tfrac{3}{10}(B_0^{(2)}/B_0^{(4)})] .$$

Analysis of the crystal-field splittings of $4f^N$ levels has shown that $B_0^{(4)}\simeq 5B_0^{(2)}$ for all lanthanides.[14] Using this ratio as a rough guide for the $5d$ splitting, we can approximate the total splitting as $\frac{1}{2}B_0^{(4)}$. For Ce^{3+}:LaF_3, then we obtain $B_0^{(4)}\simeq 30\,000$ cm^{-1} and $B_0^{(4)}/E_{df}\simeq 0.3$. Although the $4f^6 5d$ splittings of Gd^{3+}:LaF_3 have not been observed, we can safely assume that they do not differ greatly from those of Ce^{3+}:LaF_3.

Following double closure over levels of the $4f^6 5d$ configuration and a series of operator recouplings, the third-order operator acting between $^8S_{7/2}$ and ^6I_J becomes

$$+15(\tfrac{1}{35})^{1/2}E_{df}^{-2}\sum_{t,k}(-1)^{t+k}(2t+1)^{1/2}(2k+1)^{1/2}\begin{Bmatrix}1&3&2\\3&t&k\end{Bmatrix}\begin{Bmatrix}3&1&2\\4&2&t\end{Bmatrix}[\underline{E}^{(1)}(\underline{B}^{(4)}\underline{E}^{(1)})^{(t)}]^{(k)}\cdot\underline{U}^{(k)} , \tag{6a}$$

where $\underline{B}^{(k)}$ is a tensor with components equal to the coefficients of the crystal-field operator (4). Since k can be as large as 6 in expression (6a), $\Delta L,\Delta J\leq 6$ is possible, so all of the $^8S_{7/2}\rightarrow{}^6I_J$ transitions can be accommodated. Since $\underline{B}^{(k)}$ is coupled to the electric field vectors, the predicted line strengths are anisotropic.

For $^8S_{7/2}\rightarrow{}^6I_J$, $\underline{U}^{(6)}$ has by far the largest matrix elements of the various $\underline{U}^{(k)}$, so the term in (6a) for which $k=6$, $n=4$, $t=5$ dominates. The line strengths are then given by the single third-order term

$$S_{\mathrm{TPA}}(^6I_J)=\frac{50c}{11\,319}(E^4/E_{df}^2)(B_0^{(4)}/E_{df})^2 \times([^8S_{7/2}]||\underline{U}^{(6)}||[^6I_J])^2 , \tag{6b}$$

where $c=\frac{29}{60}$, 1, and $\frac{7}{15}$, respectively, for $\vec{E}\perp\hat{z}$, $\vec{E}||\hat{z}$, and circular polarization. Comparison with the predicted line strength of $^6D_{9/2}$, which owes its strength only to second-order contributions, shows $S(^6I_{7/2},\vec{E}||\hat{z})=0.006\,S(^6D_{9/2},\vec{E}||\hat{z})$ for $B_0^{(4)}/E_{df}=0.3$. A modest increase in this ratio improves the fit to the data somewhat. The closed circles in Fig. 12 were placed using the value 0.45. The intensities of the ^6I_J lines relative to one another fit very well to the ratios of $([^8S_{7/2}]||\underline{U}^{(6)}||[^6I_J])^2$, in agreement with Eq. (6b). However, the average ^6I_J line strengths are still underestimated by a factor of 5 of so. More importantly, the observed polarization dependence, which is less subject to experimental error, is misrepresented. Instead of a much smaller intensity for $\vec{E}||\hat{z}$, Eq. (6b) predicts a slightly larger intensity. Fourth-order terms alleviate the former discrepancy. To resolve the latter we must reintroduce J mixing and the third-order terms with $V=H_{\mathrm{so}}$.

Fourth-order terms with $V=H_{\mathrm{so}}$ and $V'=H_{\mathrm{CF}}$ (and vice versa) permit a direct linkage of ^8S to ^6I, which is not possible in a lower order. We can anticipate that, following triple closure over the intermediate states l,m,n in expression (1), only operators of the form $\underline{W}^{(16)k}$ need be retained in the subsequent recoupling, since these are the operators which directly link ^8S to ^6I. The values of the reduced matrix elements of these operators are shown in Table II. For $k=6$, the matrix elements are an order of magnitude larger than the intermediate coupling matrix elements $([^8S_{7/2}]||\underline{U}^{(6)}||[^6I_J])$, so there is hope that the fourth-order terms can rival the third-order terms despite the extra energy denominator. The final form of the recoupled fourth-order operator is

$$-\tfrac{2}{7}(\tfrac{13}{154})^{1/2}(\zeta_f-\zeta_d)E_{df}^{-3}(\underline{E}^{(1)}(\underline{B}^{(4)}\underline{E}^{(1)})^{(4)})^{(5)}\cdot\underline{W}^{(16)5}-\tfrac{1}{35}(\tfrac{13}{231})^{1/2}(15\zeta_f-2\zeta_d)E_{df}^{-3}(\underline{E}^{(1)}(\underline{B}^{(4)}\underline{E}^{(1)})^{(5)})^{(5)}\cdot\underline{W}^{(16)5} -\tfrac{5}{7}(\tfrac{1}{15})^{1/2}(3\zeta_f+2\zeta_d)E_{df}^{-3}(\underline{E}^{(1)}(\underline{B}^{(4)}\underline{E}^{(1)})^{(5)})^{(6)}\cdot\underline{W}^{(16)6} . \tag{7}$$

Fifth-rank as well as sixth-rank operators appear. The fifth-rank terms [the first two in (7)] have the intriguing feature that, for the hexagonal field of LaF_3, where the only fourth-rank crystal-field term in $B_0^{(4)}$, they vanish for $\vec{E}||\hat{z}$. Nevertheless, these terms cannot explain the observed anisotropy, because their numerical coefficients are much smaller than that of the sixth-rank term, which predicts the same polarization dependence as the sixth-rank third-order term (6). Furthermore, the reduced matrix elements of the fifth-rank operators are smaller than those of the sixth-rank operator (see Table II). Consequently, we can neglect the fifth-rank terms.

To compute the ^6I_J line strengths, we now add the fourth-order operator (7) to the third-order operator (6a), take the square modulus of the matrix element connecting the initial and final states, and sum over all M,M'. We find that the ratio of the fourth-order contribution (including the cross term between the third- and fourth-order terms) to the third-order contribution is very close to 1 for all ^6I_J levels for all polarizations. Thus the predicted intensity of each ^6I_J line, shown by the circled crosses in Fig. 12, is roughly doubled, but the predicted polarization dependence is the same as in third order.

To explain the anisotropy, we apply the same arguments used earlier for $^6P_{3/2}$. Using crystal-field parameters $B_0^{(6)}=1250$ cm^{-1}, $B_6^{(6)}=600$ cm^{-1}, and reduced matrix elements $(^6I_J||\underline{U}^{(6)}||^6P_{7/2})$ from Ref. 14, we find that $^6I_{7/2}$ contains the following first-order admixtures of $^6P_{7/2}$:

$$
\begin{aligned}
|\{^6I_{7/2},\pm\tfrac{1}{2}\}\rangle &= |^6I_{7/2},\pm\tfrac{1}{2}\rangle - 0.014\,|^6P_{7/2},\pm\tfrac{1}{2}\rangle\ ,\\
|\{^6I_{7/2},\pm\tfrac{3}{2}\}\rangle &= |^6I_{7/2},\pm\tfrac{3}{2}\rangle + 0.026\,|^6P_{7/2},\pm\tfrac{3}{2}\rangle\ ,\\
|\{^6I_{7/2},\pm\tfrac{5}{2}\}\rangle &= |^6I_{7/2},\pm\tfrac{5}{2}\rangle - 0.014\,|^6P_{7/2},\pm\tfrac{5}{2}\rangle \mp 0.016\,|^6P_{7/2},+\tfrac{7}{2}\rangle\ ,\\
|\{^6I_{7/2},\pm\tfrac{7}{2}\}\rangle &= |^6I_{7/2},\pm\tfrac{7}{2}\rangle - 0.000\,05\,|^6P_{7/2},\pm\tfrac{7}{2}\rangle \mp 0.016\,|^6P_{7/2},+\tfrac{5}{2}\rangle\ .
\end{aligned}
\tag{8}
$$

In an earlier paper[7] we showed that these admixtures, in themselves, could not account for the ^6I_J line strengths, thus necessitating the higher-order treatment outlined above. In particular, they underestimated the $^6I_{7/2}$ intensity for all polarizations, and by more than a factor of 100 for circular polarization. Discrepancies are similar for the other ^6I_J levels. This mechanism, in fact, predicts that ^6I_J depends in the same way as $^6P_{7/2}$ on polarization, contrary to observation. Admixtures of other levels into ^6I_J do not contribute significantly to the intensities.

Nevertheless, the $^6P_{7/2}$ admixtures play a crucial role in creating the unusual anisotropy of the ^6I_J lines. We illustrate the mechanism in detail for $^6I_{7/2}$, which, being the most isolated of the ^6I_J levels, is the least strongly J mixed. We denote the three TPA operators which contribute to these lines as $\underline{Q}^{(6)}(3)$ (third-order sixth-rank operator), $\underline{Q}^{(6)}(4)$ (fourth-order, sixth-rank operator), and $\underline{Q}^{(0)}(3)$ (third-order scalar operator acting on the $^6P_{7/2}$ ad-

TABLE IV. Matrix elements of third- and fourth-order two-photon absorption operators between components of the ground state $[^8S_{7/2},M]$ and components of the excited state $[^6I_{7/2},M']$ in Gd^{3+}. ϵ_{ij} is the coefficient of the admixture of $[^6P_{7/2},|M|=i+0.5]$ into $[^6I_{7/2},|M'|=j+0.5]$. The common factor $-2E^2/E_{df}$ has been dropped from all matrix elements.

Polarization	M,M'	$[\underline{Q}^{(6)}(3)]_{MM'}$[a]	$[\underline{Q}^{(6)}(4)]_{MM'}$[b]	$[\underline{Q}^{(0)}(3)]_{MM'}$[c]
$\vec{E}\perp\hat{z}$	$\mp\frac{3}{2},\pm\frac{1}{2}$	$-0.000\,25$[d]	-0.009[d,e]	0
	$\pm\frac{1}{2},\pm\frac{1}{2}$	$+0.000\,34$[d]	$+0.013$[d,e]	$-1.8\epsilon_{00}$[e]
	$\pm\frac{5}{2},\pm\frac{1}{2}$	$+0.000\,43$[d]	$+0.016$[d,e]	0
	$\mp\frac{1}{2},\pm\frac{3}{2}$	$-0.000\,25$[d]	-0.009[d,e]	0
	$\pm\frac{3}{2},\pm\frac{3}{2}$	$-0.000\,61$[d]	-0.023[d,e]	$-1.8\epsilon_{11}$[e]
	$\pm\frac{7}{2},\pm\frac{3}{2}$	$-0.000\,21$[d]	-0.0076[d,e]	0
	$\pm\frac{1}{2},\pm\frac{5}{2}$	$+0.000\,43$[d]	$+0.0156$[d,e]	0
	$\pm\frac{5}{2},\pm\frac{5}{2}$	$+0.000\,34$[d]	$+0.013$[d,e]	$-1.8\epsilon_{22}$[e]
	$\pm\frac{3}{2},\pm\frac{7}{2}$	$-0.000\,21$[d]	-0.0076[d,e]	0
	$\pm\frac{7}{2},\pm\frac{7}{2}$	$-0.000\,07$[d]	-0.0035[d,e]	$-1.8\epsilon_{33}$[e]
$\vec{E}\|\|\hat{z}$	$\pm\frac{1}{2},\pm\frac{1}{2}$	$+0.000\,67$[d]	$+0.025$[d,e]	$+1.8\epsilon_{00}$[e]
	$\pm\frac{3}{2},\pm\frac{3}{2}$	$-0.001\,21$[d]	-0.045[d,e]	$+1.8\epsilon_{11}$[e]
	$\pm\frac{5}{2},\pm\frac{5}{2}$	$+0.000\,67$[d]	$+0.025$[d,e]	$+1.8\epsilon_{22}$[e]
	$\pm\frac{7}{2},\pm\frac{7}{2}$	$-0.000\,14$[d]	-0.007[d,e]	$+1.8\epsilon_{33}$[e]
Circular	$-\frac{5}{2},-\frac{1}{2}$	$+0.000\,85$[d]	$+0.0313$[d,e]	0
	$-\frac{3}{2},+\frac{1}{2}$	$-0.000\,49$[d]	-0.0181[d,e]	0
	$-\frac{7}{2},-\frac{3}{2}$	$-0.000\,41$[d]	-0.0153[d,e]	0
	$-\frac{1}{2},+\frac{3}{2}$	$-0.000\,49$[d]	-0.0181[d,e]	0
	$+\frac{1}{2},+\frac{5}{2}$	$+0.000\,85$[d]	$+0.0313$[d,e]	0
	$+\frac{3}{2},+\frac{7}{2}$	$-0.000\,41$[d]	-0.0153[d,e]	0

[a] $\underline{Q}^{(6)}(3)=\frac{5}{14}(\frac{13}{35})^{1/2}E_{df}^{-1}[\underline{E}^{(1)}(\underline{B}^{(4)}\underline{E}^{(1)})^{(5)}]^{(6)}\cdot\underline{U}^{(6)}$.

[b] $\underline{Q}^{(6)}(4)=+\frac{5}{14}(\frac{1}{15})^{1/2}(5\zeta/E_{df})E_{df}^{-1}[\underline{E}^{(1)}(\underline{B}^{(4)}\underline{E}^{(1)})^{(5)}]^{(6)}\cdot\underline{W}^{(16)6}$.

[c] $\underline{Q}^{(0)}(3)=-10(\frac{2}{7})^{1/2}(\zeta/E_{df})(\underline{E}^{(1)}\underline{E}^{(1)})^{(0)}\cdot\underline{W}^{(11)0}$.

[d] Multiply by $B_0^{(4)}/E_{df}\simeq 0.4$.

[e] Multiply by $\zeta/E_{df}\simeq 0.01$.

mixture). The numerical values of the matrix elements of these three operators for ${}^8S_{7/2} \rightarrow {}^6I_{7/2}$ are listed in Table IV, which is closely analogous to Table III. The first two operators have the general form

$$\tfrac{1}{2}O^{(6)}_{-2} + \tfrac{3}{2}(\tfrac{5}{21})^{1/2}O^{(6)}_0 + \tfrac{1}{2}O^{(6)}_2 \quad \text{for } \vec{E}\perp\hat{z}\,,$$

$$3(\tfrac{5}{21})^{1/2}O^{(6)}_0 \quad \text{for } \vec{E}\|\hat{z}\,,$$

and

$$O^{(6)}_2$$

for circular polarization. In order to obtain the matrix elements of $O^{(0)}_0(3)$, the first-order ${}^6P_{7/2}$ admixtures (8) can be substituted for the $\epsilon_{MM'}$ in Table IV as a first approximation. When this is done we see at once that for $\vec{E}\|\hat{z}$, the matrix element of $O^{(0)}_0(3)$ is opposite in sign and comparable in magnitude to the sum of the matrix elements of $O^{(6)}_0(3)$ and $O^{(6)}_0(4)$ for $M'=\pm\frac{1}{2}$, $\pm\frac{3}{2}$, and $\pm\frac{5}{2}$, resulting in strong destructive interference. For $\vec{E}\perp\hat{z}$, there is constructive interference for the same M' values, thus giving rise to the pattern of anisotropy familiar from ${}^6P_{3/2}$. For $M'=\pm\frac{7}{2}$, the admixture of ${}^6P_{7/2}, M'=\pm\frac{7}{2}$ is exceedingly small in first order, and thus produces almost no interference. Since, however, the intensity of the $M'=\pm\frac{7}{2}$ component drops substantially in going from $\vec{E}\perp\hat{z}$ to $\vec{E}\|\hat{z}$, we must suppose either that in a higher-order approximation this admixture is larger (and positive in sign) or that some other admixture produces the required cancellation.

In fitting the data for ${}^6I_{7/2}$, the values of $\epsilon_{MM'}$ were allowed to vary somewhat from the first-order values (8). For $M'=\pm\frac{1}{2}$, $\pm\frac{3}{2}$, and $\pm\frac{5}{2}$, the values yielding the best fit changed by less than 35% from the first-order values. The coefficient of ${}^6P_{7/2}, M'=\pm\frac{7}{2}$ changed from -0.00005 to $+0.003$. This small value could easily arise in a higher-order approximation. The final values of the coefficients were $\epsilon_{00}=-0.011$, $\epsilon_{11}=+0.022$, $\epsilon_{22}=-0.021$, $\epsilon_{32}=+0.010$, $\epsilon_{33}=+0.003$, and $\epsilon_{23}=+0.014$ (the notation is $\epsilon_{M-0.5,M'-0.5}$). These values give the best representation of the integrated intensity as well as the individual Stark-component intensities for the two linear polarizations. The result of the fit is shown by the closed circles in Fig. 7. Mixing of the $M'=\pm\frac{5}{2}$ and $\pm\frac{7}{2}$ components was taken into account. By contrast, the horizontal lines show intensities predicted when the ${}^6P_{7/2}$ admixture is neglected. For the two linear polarizations, the Stark components are well represented, although for circular polarization, where there are no adjustable parameters, $M'=\pm\frac{3}{2}$ is 2–3 times stronger than predicted. We have found that including the effect of ${}^6P_{5/2}$ and ${}^6D_J$ admixtures or a modest presence of $B^{(4)}_2$ and $B^{(4)}_4$ crystal-field terms cannot explain the relative strength of $M=\pm\frac{3}{2}$ for circular polarization. We believe, therefore, that this small remaining discrepancy results from a small amount of J mixing with other ${}^6I_J$ levels.

The result of a similar calculation for ${}^6I_{11/2}$ is shown in Fig. 8, although because of stronger J mixing with other ${}^6I_J$ levels the final fit obtained for the Stark-component intensities is poorer. Nevertheless, we find that strong destructive interference again occurs when $\vec{E}\|\hat{z}$ for $M'=\pm\frac{1}{2}$, $\pm\frac{3}{2}$, $\pm\frac{5}{2}$, and $\pm\frac{7}{2}$. For $M'=\pm\frac{9}{2}$ and $\pm\frac{11}{2}$, $O^{(6)}_0(4)$ and $O^{(6)}_0(3)$ cannot connect these M' values to any ${}^8S_{7/2}$ components, resulting in small intensities. Corresponding constructive interference again occurs for $\vec{E}\perp\hat{z}$. Varying the first-order coefficients of the ${}^6P_{7/2}$ admixtures by a modest amount allows the intensities for the two linear polarizations to be fit more or less satisfactorily.

Despite shortcomings on some details, the interference mechanism just outlined explains the strong anisotropy of ${}^6I_{7/2,11/2}$ quite satisfactorily. For the remaining ${}^6I$ levels, the observed anisotropy of the integrated intensities can be well explained through similar calculations, even though strong J mixing prevents accurate predictions of the relative Stark-component intensities for each polarization. In fact, because of the near degeneracy of ${}^6I_{9/2}$ and ${}^6I_{17/2}$, as well as ${}^6I_{13/2}$ and ${}^6I_{15/2}$, J and M_J are no longer approximately good quantum numbers for these levels. In principle, using the eigenfunctions of a diagonalized Hamiltonian matrix which includes the crystal-field operator, even these predictions could be made accurately. The simpler calculations outlined above, however, establish the basic mechanism of the anisotropy of the ${}^6I$ lines. Consistently throughout the ${}^6I$ group, the matrix elements of $O^{(0)}_0(3)$ interfere destructively with the matrix elements of $O^{(6)}_0(3)$ and $O^{(6)}_0(4)$ for $\vec{E}\|\hat{z}$, while interfering constructively for $\vec{E}\perp\hat{z}$. The integrated intensities calculated for all the ${}^6I$ lines, neglecting J mixing among the ${}^6I$ levels and using modest adjustments of the first-order ${}^6P_{7/2}$ admixtures, are shown with $\times$'s in Fig. 12. For each ${}^6I_J$ level, the prediction of the combined third- and fourth-order contributions (the circled crosses in Fig. 12) remains unchanged for circular polarization, drops by a factor of 3–5 for $\vec{E}\|\hat{z}$, and increases by about the same factor for $\vec{E}\perp\hat{z}$ as a result of the ${}^6P_{7/2}$ admixture. With the results of these calculations, essentially every detail of the data shown in Fig. 12 has now been explained.

The above analysis of the ${}^6I$ lines suggests that their intensities should be sensitive to changes in the crystalline environment. The interference mechanism responsible for the strong anisotropy is especially sensitive to the relative magnitude of the fourth-rank and the sixth-rank crystal-field terms. Thus in different host crystals, perhaps even in the same host crystal under uniaxial pressure, significant variations in the strength of the anisotropy, as well as in the intensities relative to ${}^6P_J$ and ${}^6D_J$, can be expected.

V. CONCLUSION

The two-photon absorption spectrum of Gd^{3+} can be understood in intricate detail when third- and fourth-order terms in the perturbation series which involve spin-orbit and/or crystal-field interactions among the intermediate states are taken into account. Accurate measurements of the relative intensities and the polarization dependence of numerous two-photon transitions has established the existence, and in many cases the dominance, of these higher-order contributions. The violation of angular momentum selection rules and anomalously strong inten-

sities have been explained satisfactorily. In the LaF_3 host, strong anisotropies were shown to arise from polarization-dependent interference among second-, third-, and fourth-order terms when J mixing among the $4f^7$ levels is taken into account. In addition, the intensities of individual Stark components could in most cases be explained quantitatively, occasionally requiring revision of the Stark-component assignments derived from crystal-field calculations. In the solution, two-photon spectroscopy using two excitation beams of independently variable frequency and polarization could in principle determine the symmetry of the observed Stark components, and thereby aid in determining the structure of the hydration complex. The present results, however, were obtained with only a single excitation beam.

Higher-order contributions should be widely encountered in the two-photon spectra of other rare-earth, as well as actinide, ions because the excited configurations occur at lower energies than in Gd^{3+}. We have recently completed a study of the two-photon spectrum of Eu^{2+} in CaF_2, SrF_2, and BaF_2 lattices, where the $4f^6 5d$ configuration lies dramatically lower than in the isoelectronic Gd^{3+} ion. The sharp $4f^7$ excited states, in fact, are embedded in the broad intense $5d$ bands, and can be observed only by two-photon absorption, which suppresses the broad background through the parity-selection rule. Fritzler and Schaak[4] identified $^6P_{7/2,5/2}$ in this fashion. We have observed the ^6I and ^6D groups as well. The smaller average energy denominator indeed enhances the relative intensity of many levels which owe their strength to third- and fourth-order contributions, although the greater relative energy spread of the intermediate levels partly invalidates the closure approximation, and complicates the theoretical description. The results of this study will be published in a planned forthcoming paper.

ACKNOWLEDGMENTS

It is a pleasure to thank Professor N. Bloembergen for providing the stimulus for this work and for numerous valuable suggestions throughout the course of the research. We appreciatively acknowledge receiving a preliminary unpublished version of the paper of B. R. Judd and D. R. Pooler prior to publication, and one of us (M.C.D.) wishes particularly to thank Professor B. R. Judd for a number of stimulating discussions. One of us (A.B.) acknowledges financial support from Laboratoire de Spectroscopie et d'Optique du Corps Solide, associé au C.N.R.S. No. 232, Université Louis Pasteur, Strasbourg, France. This research was supported by the U.S. Joint Services Electronics Program under Contract No. N00014-75-C-0648.

---

*Present address: Bell Laboratories 4D515, Holmdel, NJ 07733.
†Present address: Central Research Division, Varian Associates, Palo Alto, CA 94303.

[1]W. Kaiser and C. G. B. Garrett, Phys. Rev. Lett. 7, 229 (1961).
[2]E. Bayer and G. Schaak, Phys. Status Solidi 41, 827 (1970).
[3]P. A. Apanasevich, R. I. Gintoft, V. S. Korolkov, A. G. Makhanek, and G. A. Skripko, Phys. Status Solidi B 58, 745 (1973); A. G. Makhanek and G. A. Skripko, Phys. Status Solidi A 53, 243 (1979).
[4]U. Fritzler and G. Schaak, J. Phys. C 9, L23 (1976); U. Fritzler, Z. Phys. B 27, 289 (1977).
[5]W. M. Yen, C. G. Levey, S. Huang, and S. T. Lai, J. Lumin. 24-25, 659 (1981).
[6]M. Dagenais, M. Downer, R. Neumann, and N. Bloembergen, Phys. Rev. Lett. 46, 561 (1981).
[7]M. C. Downer, A. Bivas, and N. Bloembergen, Opt. Commun. 41, 335 (1982).
[8]M. C. Downer, Ph.D. thesis, Harvard University, 1983 (unpublished).
[9]B. R. Judd and D. R. Pooler, J. Phys. C 15, 591 (1982).
[10]B. R. Judd, Phys. Rev. 127, 750 (1962).
[11]G. S. Ofelt, J. Chem. Phys. 37, 511 (1962).
[12]J. D. Axe, Jr., Phys. Rev. 136, A42 (1964).
[13]W. T. Carnall, P. R. Fields, and B. G. Wybourne, J. Chem. Phys. 42, 3797 (1965); W. T. Carnall, P. R. Fields, and K. Rajnak, *ibid.* 49, 4412 (1968).
[14]W. T. Carnall, H. Crosswhite, and H. M. Crosswhite (unpublished), of Argonne National Laboratories have made a compilation of energy level structure and transition probabilities in the spectra of trivalent lanthanides in LaF_3. Copies of this unpublished compilation are available from its authors upon request.
[15]D. A. Jones, J. M. Baker, and D. F. D. Pope, Proc. Phys. Soc. London 74, 249 (1959).
[16]R. P. Baumann and S. P. S. Porto, Phys. Rev. 161, B42 (1967).
[17]A. K. Cheetham, B. E. F. Fender, H. Feuss, and A. F. Wright, Acta Crystallogr. Sect. B 32, 94 (1976).
[18]Q. Munir, E. Wintner, and A. J. Schmidt, Opt. Commun. 36, 467 (1981).
[19]L. Swofford and W. M. McClain, Chem. Phys. Lett. 34, 455 (1975).
[20]J. P. Hermann and J. Ducuing, Phys. Rev. A 5, 2557 (1972).
[21]G. Koren, C. Cohen, and W. Low, Solid State Commun. 16, 257 (1975).
[22]R. L. Schwiesow and H. M. Crosswhite, J. Opt. Soc. Am. 59, 602 (1969).
[23]W. T. Carnall, P. R. Fields, and R. Sarup, J. Chem. Phys. 54, 1476 (1971).
[24]R. L. Schwiesow and H. M. Crosswhite, J. Opt. Soc. Am. 59, 592 (1969).
[25]J. F. Giuliani, Opt. Lett. 3, 149 (1978).
[26]D. G. Miller, J. Am. Chem. Soc. 80, 3576 (1957).
[27]S. Freed, Rev. Mod. Phys. 14, 105 (1942).
[28]E. V. Sayre, D. G. Miller, and S. Freed, J. Chem. Phys. 26, 109 (1957).
[29]D. R. Svoronos, E. Antic-Fidancev, M. Lemaitre-Blaise, and P. Caro, Nouv. J. Chim. 5, 547 (1981).
[30]L. Couture, J. Lumin. 18-19, 891 (1979).
[31]C. K. Jorgensen, Prog. Inorg. Chem. 4, 73 (1962).
[32]W. M. Yen, W. C. Scott, and A. L. Shawlow, Phys. Rev. 136, A271 (1964).
[33]A. Habenschuss and F. H. Spedding, J. Chem. Phys. 70, 2797 (1979); *ibid.* 70, 3758 (1979); *ibid.* 73, 442 (1980).

[34]T. Mioduski and S. Siekierski, J. Inorg. Nucl. Chem. 37, 1647 (1975).

[35]P. R. Monson and W. M. McClain, J. Chem. Phys. 53, 29 (1970); W. M. McClain, *ibid.* 55, 2789 (1971).

[36]M. Göppert-Mayer, Ann. Phys. (Leipzig) 9, 273 (1931).

[37]J. Hougen and S. Singh, Phys. Rev. Lett. 10, 406 (1963); Proc. R. Soc. London Ser. A 277, 193 (1964).

[38]B. R. Judd, *Second Quantization in Atomic Spectroscopy* (The John Hopkins Press, Baltimore, 1967).

[39]B. R. Judd, *Operator Techniques in Atomic Spectroscopy* (McGraw-Hill, New York, 1963).

[40]The operators (5a) and (5b) differ by a factor of -2 from results stated in Ref. 9. The discrepancy arises from an error in converting the dipole operator $\vec{D}$ to second quantized form in that paper. The correct second quantized form of this operator is:

$$\vec{D}=(2)^{1/2}[(f^{+}d)^{(01)}-(d^{+}f)^{(01)}]\ ,$$

where the symbols are defined in Ref. 9. The change increases calculated absolute cross sections by a factor of four, but does not affect calculated relative cross sections nor any theoretical conclusions derived in Ref. 9.

[41]A. R. Edmonds, *Angular Momentum in Quantum Mechanics* (Princeton University Press, Princeton, 1960).

[42]W. S. Heaps, L. R. Elias, and W. M. Yen, Phys. Rev. B 13, 94 (1975).